Chem Soc Rev

Using lanthanide ions in molecular bioimaging

Journal:	*Chemical Society Reviews*
Manuscript ID:	CS-REV-09-2014-000293.R1
Article Type:	Review Article
Date Submitted by the Author:	03-Dec-2014
Complete List of Authors:	Pope, Simon; University of Cardiff, School of Chemistry Amoroso, Angelo; Cardiff University,

Using lanthanide ions in molecular bioimaging

Angelo J. Amoroso* and Simon J.A. Pope*

School of Chemistry, Main Building, Cardiff University, Park Place, Cardiff, Wales, UK CF10 3AT.

Abstract

Trivalent lanthanide ions offer remarkable opportunities in the design of bioimaging agents: this review presents an accessible discussion of their application in both optical and magnetic resonance imaging. Aspects of molecular design, control over key physical properties and biological compatibility are discussed in this context, together with developments and opportunities as responsive probes and in multimodal imaging.

1. Introduction

In recent years, a number of highly informative and comprehensively inclusive reviews have been written addressing the areas of luminescence and magnetic resonance imaging (MRI).[1] Furthermore, some of these reviews have focussed on the use of lanthanides ions in these applications.[2] With this in mind, this review aims to introduce the general reader (in particular undergraduate and graduate students) to the area of lanthanide ions for luminescence and/or MRI applications, clarify some general misconceptions and give an indication of current directions in these areas of research. The subject area is far too broad for this review to be comprehensive[3] and we have chosen only illustrative examples of molecular probes for the reader; we can only apologise to the authors of other excellent examples that we have omitted. At times the subject topic will also reference apparently daunting

physical equations. We have, where possible, tried to avoid such references and instead explain their relevance to the chemist involved in the design and synthesis of such compounds. The discussion will cover optical properties and luminescence imaging applications, MRI and finally the opportunities offered in multimodal imaging.

2. Luminescence Imaging with Lanthanide Ions

Fluorescence microscopy is a rapidly developing optical imaging technique ideal for analysing biological samples at high resolution such that individual cells can be imaged. Diffraction-limited microscopy has an image resolution of *ca.* 200-250 nm; further developments in hardware and software facilitate super-resolved fluorescence microscopy at *ca.* 20-100 nm image resolution (an area recognised with the 2014 Nobel Prize in Chemistry[4]), rendering sub-cellular components in remarkable detail. Fluorescent organic molecules dominate the commercial market for cell imaging agents, with a wide range of labels and fluorescent proteins available, although biocompatible quantum dots are also gaining in popularity. For luminescent molecules, the absorption and emission wavelengths (λ_{abs} and λ_{em}), observed lifetime (τ_{obs}) and the quantum yield (ϕ) are key physical parameters that describe the luminescence. Typically the emitted photon possesses a lower energy than the absorbed photon ($\lambda_{abs} < \lambda_{em}$) and this difference in wavelengths is defined as the Stokes' shift. Consideration of these parameters is critical to the application of luminescent molecules in biological imaging. However, there are significant photophysical and biological advantages to the use of *f*-metal ion coordination complexes in such applications. In particular, exciting

opportunities are afforded by luminescent Ln(III)-based systems (large Stokes' shifts; long luminescent lifetimes > 1ms) and this section will discuss some of the key developments that have allowed their application.[5]

Relevant Microscopy Applications

Confocal fluorescence microscopy (CFM) is a powerful optical technique that makes use of luminescence (in this case the term *fluorescence* is misleading as *phosphorescence* can also be utilised in CFM) to generate the image. It is possible to obtain confocal fluorescence microscopes with a range of different light excitation sources (*e.g.* lamps, lasers and LEDs), which, together with suitable optics, can deliver a monochromated wavelength to the sample. The use of NIR light allows better light penetration and improved imaging depth.[6] Multi-photon excitation sources are now also available, potentially allowing low energy (*e.g.* NIR) irradiation of samples. For reference, the two-photon absorption (TPA) cross section is defined as $\sigma_{2PA}(\lambda)$ and given in GM (where GM = Goeppert-Mayer unit; 10^{-50} cm^4 s per photon per molecule). The magnitudes of two- and three-photon cross sections thus determine the required light intensity for excitation and may constrain bioapplicability of a given probe; typical TPA values for organic chromophores are 10-100 GM, but higher TPA cross-sections facilitate lower irradiating light intensities.[7] Significant progress has been made in recent years with the utility of Ln(III) complexes and optimized cross-sections.[8,9,10]

Fluorescence lifetime imaging microscopy (FLIM) is a more advanced form of the technique and creates the image based on the emission lifetime rather than the intensity of the signal. A pulsed light source is required and

FLIM commonly employs time-correlated single-photon counting (TCSPC); modern microscopes can have picosecond resolution. The principal advantage of FLIM is that it can deliver quantitative information since the lifetime of the probe is independent of its concentration, providing measurement of dynamic events and an ability to monitor cellular compartments with good spatial resolution.[3] The equivalent approach that makes explicit use of phosphorescent probes, such as relevant metal complexes, is termed PLIM. In a subtle variation, gated microscopy allows the luminescence signal to be collected after a prescribed time delay, which is particularly useful for removing short-lived fluorescence (τ < 20 ns) from endogenous (biological) fluorophores.

A brief description of lanthanide ion luminescence

Upon irradiation (Scheme 1) with an appropriate wavelength, a light-absorbing species (termed the *antenna*) will convert to its singlet electronically excited state (S_1); radiative decay from this state can occur *via* fluorescence (*i.e.* the molecule is a fluorophore) and is typically short-lived (commonly < 50 ns). Alternatively, intersystem crossing (ISC; mediated by a number of processes including spin-orbit coupling and heavy atom effects) can generate the lower lying triplet excited state (T_1). This is a spin-forbidden process since $\Delta S \neq 0$ and radiative decay from the triplet state to the ground state is slow, occurring *via* phosphorescence. Due to the spin-forbidden nature of the radiative relaxation, the T_1 state can be very long-lived and susceptible to other non-radiative processes, including quenching by molecular oxygen.

Ln(III)	Ground state	Emitting state	λ_{em} region	Nature of emission
Pr	$^3H_4$	$^1D_2$, $^3P_0$	Vis. and NIR	Phos. and fluor.
Nd	$^4I_{9/2}$	$^4F_{3/2}$	NIR	Fluor.
Sm	$^6H_{5/2}$	$^4G_{5/2}$	Vis.	Phos.
Eu	$^7F_0$	$^5D_0$	Vis.	Phos.
Gd	$^8S_{7/2}$	$^6P_{7/2}$	UV	Phos.
Tb	$^7F_6$	$^5D_4$	Vis.	Phos.
Dy	$^6H_{15/2}$	$^4F_{9/2}$	Vis.	Phos.
Ho	$^5I_8$	$^5S_2$, $^5F_5$	Vis. and NIR	Fluor.
Tm	$^3H_6$	$^1D_2$, $^1G_4$, $^3H_4$	Vis.	Phos.
Yb	$^2F_{7/2}$	$^2F_{5/2}$	NIR	Fluor.

Table 1. Basic information on the electronic transitions responsible for Ln(III) luminescence.

Most luminescent organic molecules emit light without any change in spin-state (*i.e.* $S_1 \rightarrow S_0$; fluorescence), and thus generally possess relatively small Stokes' shifts (*e.g.* < 3000cm^{-1}). However, the luminescence from Ln(III) ions originates from 4*f*-4*f* transitions, which are often sharp in appearance and are identifiably characteristic of the specific ion; emission can occur in the UV, visible or NIR regions (Table 1). The intraconfigurational 4*f*-4*f* transitions are formally forbidden, and thus possess very low molar absorptivities (ε) limiting direct excitation, although a number of mechanisms (coupling with vibrational modes, *J*-state mixing and overlap with 5*d* orbitals and charge transfer states) can partially relax the (electric dipole) selection rules. The established strategy for overcoming this is to incorporate a sensitizing chromophore (also referred to as the *antenna*), which absorbs light and transfers energy to the 4*f* excited state *via* a mechanism that often involves the T_1 state of the sensitizer (Scheme 1). As a consequence of this mechanism the Stokes' shift can be much larger than simpler organic systems, and is a function of the particular

pathway for populating the 4*f* excited state. The overall quantum yields of emissive Ln(III) complexes depend on the sensitivity of 4*f*-centred excited states to O-H, N-H and C-H vibrational oscillators (particularly for the NIR emitting lanthanides), providing efficient non-radiative deactivation pathways (k_{nr}) and should be suppressed to enhance the emission, and the efficiency of energy transfer between the antenna and lanthanide ion. [11]

The forbidden nature of the 4*f*-4*f* transitions results in slow relaxation from the Ln(III) emitting state and thus long observed lifetimes (τ_{obs}). For aqueous solutions of DOTA-type Eu(III) and Tb(III) complexes, typical τ_{obs} values are *ca.* 1 ms; for NIR emitting Yb(III) and Nd(III) these values drop to *ca.* 1 μs and < 1 μs, respectively. Er(III) emission is extremely sensitive to quenching by O-H, N-H, C=O and C-H oscillators [12, 13] and is very rarely observed in protic media. [14] A critical advance in Ln(III) luminescence spectroscopy has been the use of time-resolved lifetime measurements in water and deuterated water (one assumes that O-D oscillators contribute minimally to k_{nr}) to approximate the inner sphere hydration (termed '*q*') at Ln(III).[15] Equations, which include both inner and outer sphere contributions, for the determination of *q* are known for Nd(III), Sm(III), Eu(III), Tb(III), Dy(III) and Yb(III) and have been summarised elsewhere.[11] Care should be taken in the interpretation of calculated *q* values since errors are often significant (*q* ±0.5). Of importance in this discussion is the fact that inner sphere hydration plays a very important role in determining the water proton relaxivity of a given Gd(III) complex (Section 3). Therefore it is common practice, for a given ligand, to isolate both luminescent Eu(III) and the analogous Gd(III) species,

allowing correlation between luminescence and relaxometric assessments with respect to understanding lanthanide hydration.

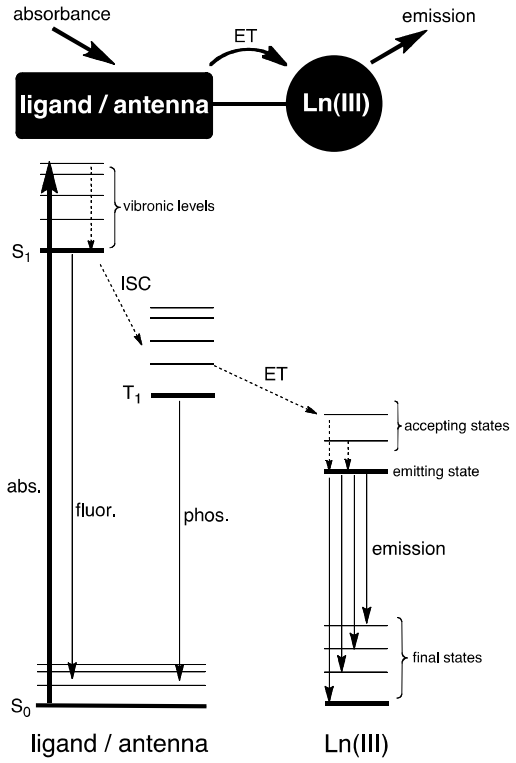

Scheme 1. Top: simplified model for describing a common mechanism for sensitized lanthanide luminescence. Bottom: typical energy level diagram for an emissive chromophore-appended lanthanide complex sensitized via a ligand-centred triplet excited state (abs = absorbance; fluor. = fluorescence; phos. = phosphorescence; ISC = intersystem crossing; ET = energy transfer).

From an imaging perspective the antenna group defines λ_{abs} and is a key component to consider in the design of Ln(III)-based agents' compatibility with CFM excitation sources. For Eu(III) ($^5D_0$ ~17200 cm^{-1}) and Tb(III) ($^5D_4$ ~20400 cm^{-1}), the triplet state of the antenna must lie >2000 cm^{-1} above the accepting Ln(III) state to allow sensitization and prevent back energy transfer (which can result in lowered emission intensity from the Ln(III)); a wide range of sensitising chromophores have been studied.[11]

Suitable antennae for Eu(III) and Tb(III) are commonly based upon polyaromatic or heterocyclic species, which absorb between 350-410 nm, and possess small singlet-triplet energy gaps. For NIR emitting Ln(III) such as Yb(III) ($^2F_{7/2}$ ~10200 cm^{-1}) the range of antennae is obviously broadened, with great imagination being applied to such systems that can range from donor-acceptor organics to transition metal complex moieties. Figure 1 shows the structures of some reported antennae for sensitized emission; whilst acetophenone and naphthyl-type chromophores are good sensitisers for a wide range of Ln(III), it should be noted that pyrene, anthracene and anthraquinone antennae all possess triplet levels that lie below the accepting states of Eu(III) and Tb(III) and are better suited, therefore, to NIR emitting ions which possess lower lying accepting states.

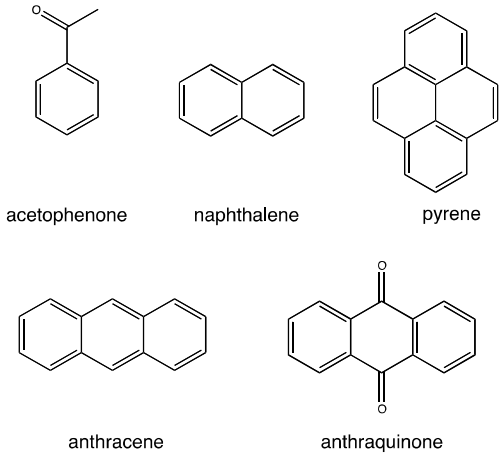

Figure 1. Examples of sensitising aromatic chromophores (antennae).

For imaging purposes Ln(III) complexes are also advantageous because of the dependence of the emission spectral form and lifetime on the coordination environment. Eu(III) is the exemplar in this context with sharp emission bands arising from $^5D_0 \rightarrow {}^7F_J$ (J = 0,1,2,3,4) that are subtly sensitive to the nature

and type of ligand donor and the coordination geometry at the ion. These properties enable the rational design of responsive probes (also referred to as sensors) where binding events at the Ln(III) ion can be interrogated directly using luminescence methods and ratiometric analyses (*i.e.* independent of probe concentration). For example, Ln(III) ions have a strong affinity for anions and direct binding to the Ln(III) ion typically occurs through a reversible intermolecular process (Scheme 2), inducing reversible displacement of coordinated water molecules (*i.e. q* is reduced) resulting in measurable changes in luminescent output (*e.g.* relative and integrated intensities, and lifetime). An appreciation of anion binding affinities and the resultant perturbation of the Ln(III) luminescence are very important in a biological context since various endogenous anionic residues are available for binding.

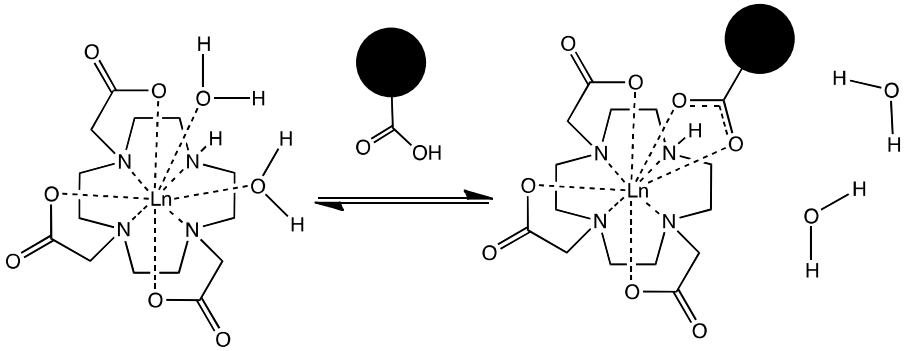

Scheme 2. Coordinative interaction of an anionic residue with a hydrated Ln(III)-DO3A complex.

Bioprobes based upon Ln(III) species must obviously possess the necessary physical properties to allow their application: water solubility, thermodynamic stability at physiological pH and kinetic inertness, photostability and minimal cytotoxicity are all highly desirable criteria.

2.1 Lanthanide complexes as imaging labels

Prior to their deployment in cell imaging studies, luminescent lanthanide complexes, particularly based on Eu(III), had clear precedent as optical labels through their use, over a number of decades, in sensitive bioanalyses such as DELFIA (dissociation-enhanced lanthanide fluorometric immunoassay). [16] More recently, luminescent macrocyclic Eu(III) complexes have been used to image and assess the extent of bone structure damage (microcracks). An amido-naphthalene group acts as the antenna and peripheral acetate groups target exposed Ca(II) sites of the hydroxyapatite lattice of the bone. CFM (Figure 2) provided far greater fine detail of the bone surface morphology, through the observation of Eu(III)-based red emission and improved signal contrast. [17]

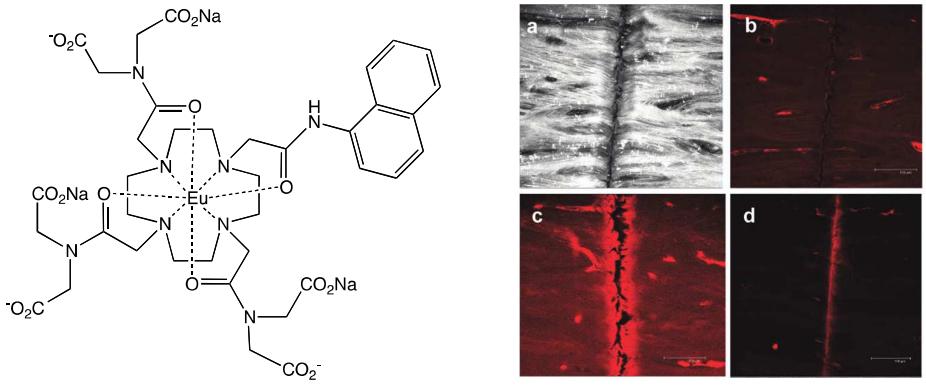

Figure 2. A polycarboxylate terminated Eu(III) complex (left) and microscopy images of bone sample immersed in 10^{-3} M solution of the complex. (a) reflected light image: 0 h; (b) control; (c) 4 h; (d) 24 h. Reprinted with permission from McMahon et al, *J. Am. Chem. Soc.*, 2009, **131**, 17542. Copyright 2009 American Chemical Society.

Macrocyclic Ln(III) complexes can be successfully applied to time-resolved luminescence microscopy, as shown by comparing small diameter silica particles labelled either with cationic complexes of phosphorescent Eu(III) (Figure 3) or rhodamine 6G (a fluorophore with a short fluorescence lifetime), which emits at similar wavelengths to Eu(III). The microscopy demonstrated that a microsecond time-delay allowed the Eu(III)-labelled silica particles to be easily differentiated from those labelled with rhodamine 6G.[18]

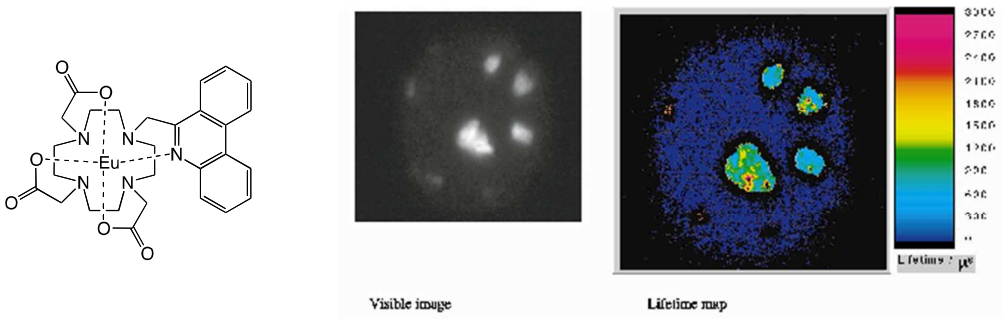

Figure 3. Structures of the complexes (left) and a visible image and lifetime map for the Eu-DO3A derived complex loaded onto silica suspended in water. Reprinted with permission. Copyright 2000 Elsevier.

Bünzli and co-workers have described an alternative class of luminescent complex: bimetallic, triple-stranded helical species of the general formula $[Ln_2L_3]$ (Figure 4) that form through self-assembly.[19] Both Ln(III) ions are tightly bound in a nonadentate coordination sphere, which limits any interaction with water. The complexes can be bioconjugated with avidin or monoclonal antibodies, allowing recognition of proteins expressed on the surface of breast cancer cells. These systems can be applied to 'on-chip' immunohistochemical detection methodologies.[20]

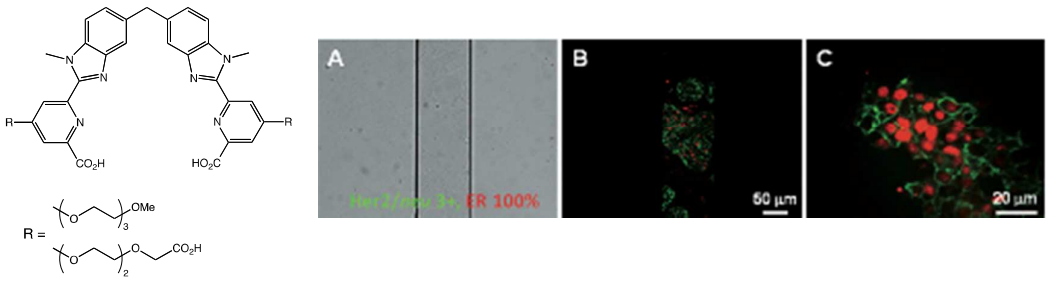

Figure 4. Ligands (left) for bimetallic helical complexes, and 'on-chip' immunohistochemical detection of Her2/neu and ER in a breast cancer tissue sample. (A) Bright field image; (B) merged luminescent image, Her2/neu detected by a green-emitting Tb(III) complex and ER stained with a red-emitting Eu^{III} complex; (C) magnified image.

2.2 Cellular Imaging with macrocyclic lanthanide complexes

Both 1,3,5-triazacyclononane (TACN) and 1,4,7,10-tetraazacyclononane (cyclen) provide excellent ligand scaffolds for the development of Ln(III) based cell imaging agents, yielding complexes with high stability and kinetic inertness.

Parker and co-workers have investigated the cellular imaging ability of a wide range of monometallic Ln(III)-based probes based on cyclen derivatives of Eu(III) and Tb(III).[21] Each complex possesses a sensitizing chromophore (Figure 5; *e.g.* tetraazatriphenylene, azaxanthone, azathiaxanthone), which is covalently linked to the cyclen framework. The periphery of the ligand architectures can be designed to dictate overall charge, influence lipophilicity and control cellular localisation.

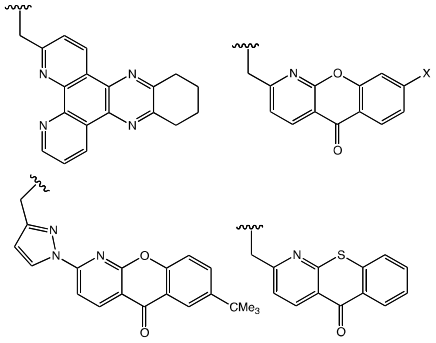

Figure 5. Examples of aromatic sensitizing chromophores used for CFM.

The dominant mechanism of cellular uptake for these cyclen complexes is macropinocytosis (the formation of large endocytotic vesicles of irregular shape and size). The nature and linkage of the sensitizing chromophore is an important factor in determining cellular uptake and localization. The intracellular localization profile that is observed for the majority of these macrocyclic Ln(III) complexes is endosomal-lysosomal (confirmed through co-staining experiments with LysoTracker); generally the rates of uptake and egress are fast. Complexes that localized in the mitochondria (Figure 6) for long periods of time (up to 10 hrs) demonstrated lower IC_{50} values (higher cytotoxicity).

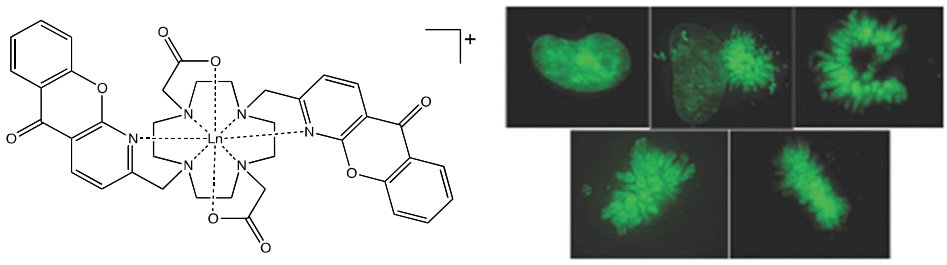

Figure 6. The chromophorically 1,7-substituted complex (left) and a time course (5 min intervals) of microscopy images staining chromatin in a cell undergoing division (HeLa cells, Ln = Tb(III) complex, λ_{ex} = 300 nm).

Monocationic Ln(III) complexes utilising azaxanthone-type chromophores in the 1- and 7-positions of the cyclen ring (Figure 6) have shown selective staining of chromosomal DNA in dividing cells.[22] The complexes possess low cytotoxicity (IC_{50} >400μM), but single-photon illumination induces phototoxicity. Two-photon absorption may reduce such phototoxic effects.

Substituents added to an azaxanthone sensitizer dramatically influence the *in cellulo* trafficking behaviour of the probe. Simple structural changes that tune amphiphilicity reveal an element of control over cellular uptake, trafficking, localization and toxicity. More complex targeting vectors (Figure 7) can also be conjugated to the azaxanthone antenna: peptide conjugates promote rapid internalization and cytosolic localisation; lipophilic oligo-guanidinium vectors induced apoptotic cell death (IC_{50} 12 μM) following localization within mitochondria.

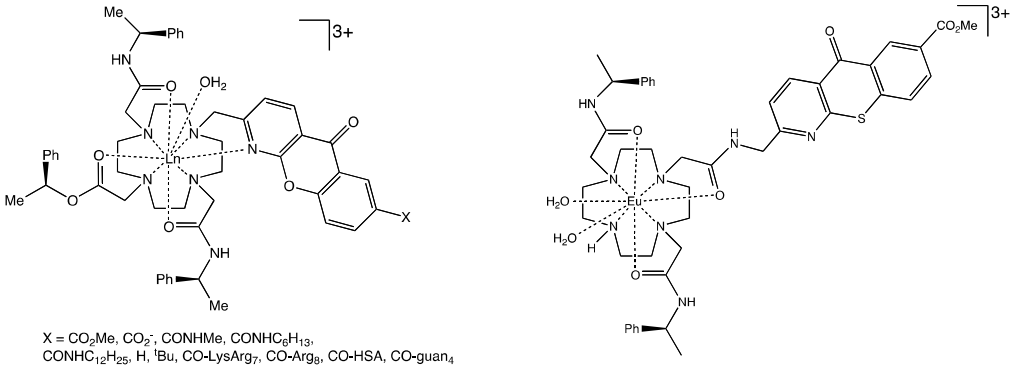

Figure 7. Left: Functionalising the periphery of the *N*-coordinated azaxanthone chomophore: hydrophilic (X = carboxylate and carboxamide),

lipophilic (X = tertiary butyl, alkyl) and bio-inspired (X = LysArg, HSA, guan) variants. Right: An example of a mitochondrial localizing Eu-based probe.

With appropriate design, such complexes lend themselves to analytical approaches in a biological context. The ratiometric luminescence characteristics of Eu(III) $^5D_0 \rightarrow {}^7F_J$ (J = 0,1,2,3,4) can be exploited, using hyper-spectral analysis of microscopy images, to signal changes in intracellular biochemical species in real time. Eu(III) complexes (Figure 7, right) that reversibly bind bicarbonate indicate a mitochondrial bicarbonate concentration of 10-30 mM.[23]

Alternative chromophores based on a pyridylalkynylaryl group combine well with Eu(III) to provide high molar absorption coefficients and efficient sensitisation (Figure 8). For example, a series of functionalised dipicolinate ligands react with Ln(III) to give tris-chelate complexes of the form $[Ln(L)_3]^{3-}$. The absorption properties of the ligands can be tuned through the degree of charge transfer character imparted by the aryl substituent.[24] Selected Eu(III) complexes of this type possess marked two-photon absorption cross-section values (775 GM at 740 nm excitation) in dichloromethane (note that such complexes usually dissociate in aqueous solutions).[25]

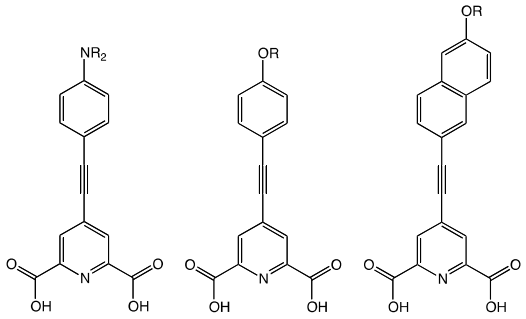

Figure 8. Examples of donor-substituted dipicolinate ligands.

To address biocompatibility, a cyclen-based Eu(III) complex (Figure 9) incorporates both a pyridylalkynylaryl chromophore and two peptide sequences for targeting Cyclin A (needed for stem cell cycle progression). The chromophore enables two-photon absorption at 12 GM, which increased to 68 GM when the complex was bound to Cyclin A allowing cell imaging in live HeLa cells using two-photon confocal microscopy (λ_{ex} = 800 nm).[26]

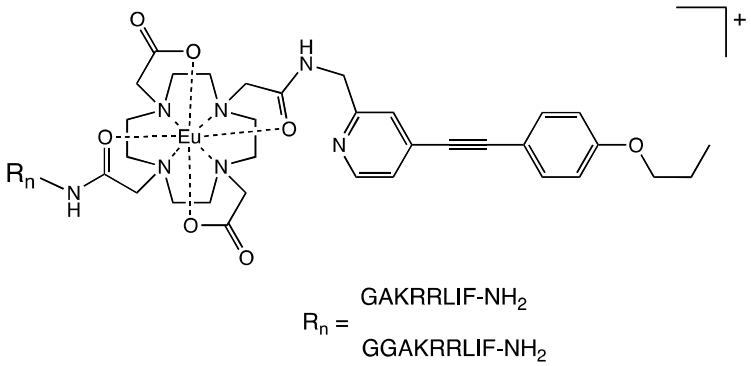

Figure 9. A Eu(III) complex incorporating a pyridylalkynylaryl chromophore.

As discussed earlier, complexes based upon the cyclen framework have clearly yielded a significant range of Ln(III) imaging agents of great utility, the broader application of such species are often hampered by their intrinsically poor brightness, where brightness, *B*, is defined as $B(\lambda) = \varepsilon(\lambda)\phi$ (where ε = molar absorption coefficient; ϕ = quantum yield). This limitation has been tackled through the design of tris-chromophoric derivatives of triazacyclononane (TACN) that bind the Ln(III) tightly and limit the approach of water solvent. Eu(III) complexes of TACN with three *para*-substituted pyridyl-alkynylaryl groups can possess impressive quantum yields (up to 50%) and large molar absorption coefficients (> 50000 $M^{-1}cm^{-1}$) leading to very bright

emission, even in aqueous solution. Although pyridylalkynylaryl groups possess λ_{max} at 310-340 nm, the magnitude of the absorption coefficient allows CFM with λ_{ex} = 355 and 365 nm. The emission lifetimes of the Eu(III) complexes are typically around 1 ms, allowing time-gated (at 10 μs) images to be obtained.[27]

Variations in this core structural motif have allowed the development of a range of Eu(III)-based probes. A phosphinate-derived Eu(III) complex (Figure 10) has shown selectivity for staining mitochondria. Such complexes can be utilised as donor components in FRET (fluorescence resonance energy transfer) bio-assays, wherein the quenching of the Eu(III) signal is indicative of intermolecular energy transfer to an accepting near-IR dye (*e.g.* cyanine dye).

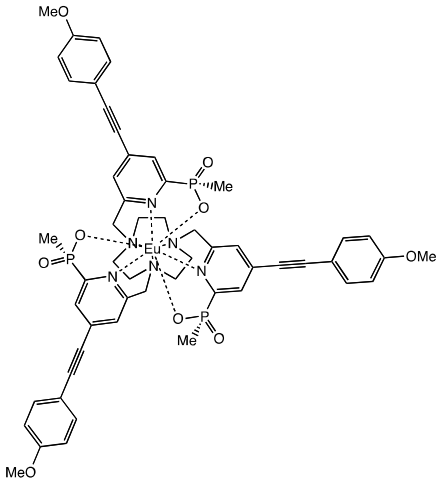

Figure 10. A mitochondrial staining Eu(III)-TACN complex.

The culmination of these different studies has resulted in the development of 'EuroTracker' dyes, variants of which are shown to give selective illumination of mitochondria, lysosomes or endoplasmic reticulum (ER).[28]

2.3 Bioimaging using multi-photon excitation sources

The two-photon sensitization and imaging of a water-soluble Eu(III) complex has been reported with substituted 2,6-pyridinedicarboxylic acid type ligands (Figure 11); the complex was surprisingly stable and strongly emissive in water (ϕ ~16%) with a long lifetime (1.06 ms). T24 cancer cells were incubated with the complex and imaged using two-photon excitation at 760 nm (σ_{2PA}(760) = 19 GM). Intracellular localization in the perinuclear region and the nucleus (which could be indicative of nucleoli targeting) was observed (Figure 11).[29]

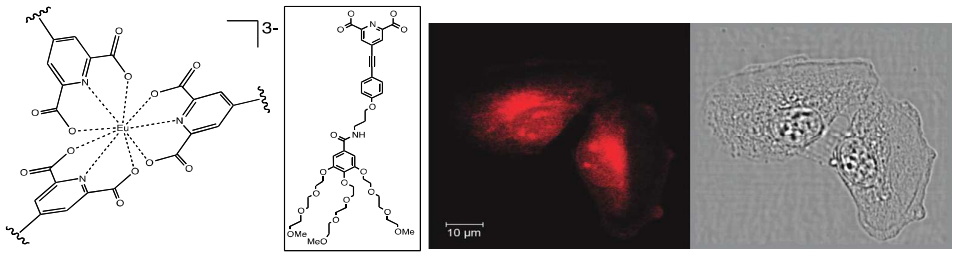

Figure 11. The tris-picolinate complex core (left), with free ligand shown Inset. Two-photon excited luminescence (left, λ_{ex} 760 nm) and phase contrast (right) images of T24 cancer cell fixed in ethanol and loaded with $[Na]_3[Eu(L)_3]$. Reprinted with permission from Picot et al, *J. Am. Chem. Soc*., 2008, **130**, 1532. Copyright 2008 American Chemical Society.

The development of acyclic ligand systems for Ln(III) ions has run in parallel with those myriad macrocyclic derivatives described earlier. In this context, Bünzli's self-assembled, triple-stranded helical complexes of the general form $[Ln_2L_3]$ can be adapted for biological study. The hydrophilicity of these complexes can be controlled through the addition of polyoxoethylene chains to the ligand periphery (Figure 12). [30] Similar approaches also allow

bioconjugation and an element of control over cell permeability. The advantageous absorption and emission properties of the $[Eu_2L_3]$ species (excitation wavelengths tuned towards 400 nm, good quantum yields and long millisecond lifetimes in water) have allowed their application in CFM.

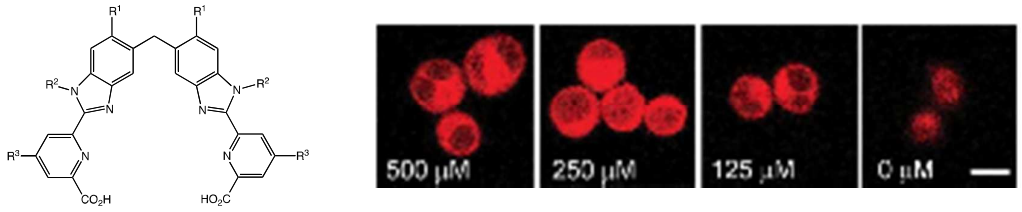

Figure 12. Ligand utilized for the bimetallic helicate $[Eu_2L_3]$ (R^1 = H, R^2 = Me, R^3 = PEG chain). Cells were incubated in presence of different concentrations of the helicate in RPMI-1640 for 24 h. The images were taken using a Zeiss LSM 500 META confocal microscope (λ_{ex} 405 nm).

Cancerous (HeLa, MCF-7, HaCat) and non-cancerous (Jurkat) cell lines have been investigated in the imaging studies. Uptake was generally defined through endocytosis with the Eu(III) complexes showing staining of the cytoplasm and liposomes of the ER.[31] These complexes have also been applied to multi-photon excitation, with both two-photon (Figure 13) and three-photon absorption exploited in an imaging context.[32] Multi-photon absorption allows the use of longer wavelength excitation (*e.g.* NIR), which is more attractive when considering the optical window of biological material, and thus improving the depth of light penetration and resolution of 3D images.[4]

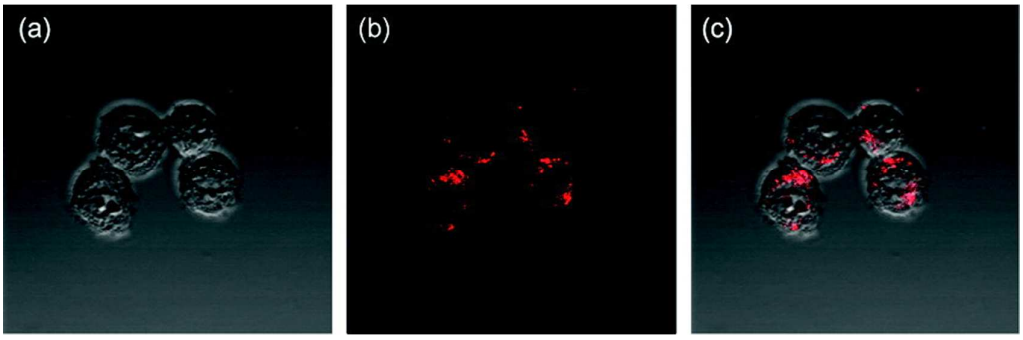

Figure 13. Two-photon microscopy images of HeLa cells incubated with 200 μM of a bimetallic Eu(III) helicate in RPMI-1640 culture medium for 12 h at 37 °C, 5% CO_2: (a) bright field image; (b) luminescence (λ_{ex} = 750 nm, λ_{em} = 570−650 nm); (c) merged image. Reprinted with permission from Eliseeva et al, *J. Phys. Chem. B*, 2010, **114**, 2932. Copyright 2010 American Chemical Society.

The significant potential of microscopy that utilises both NIR excitation and and NIR emission[33] has been demonstrated through the use of TPA of Yb(III)-containing probes with either 2,6-substituted pyridine ligands or TACN based scaffolds, as described earlier for Eu(III); the antenna component in both cases is an pyridylalkynylaryl unit. In this case TPA sensitized Yb(III) emission required irradiation at 700-900 nm that populates the ILCT excited states of the antenna. Mouse brain slices were successfully imaged using a bespoke microscope set-up allowing two-photon NIR irradiation (760 nm) with detection at 1000 nm (corresponding to the Yb(III) $^2F_{5/2} - {}^2F_{7/2}$ transition).[34]

2.4 Luminescent sensors in bioimaging

The advantageous use of luminescent Ln(III) complexes as chemosensors[35] (*i.e.* responsive systems) has been elegantly demonstrated in a biological context for targeting and imaging intracellular zinc. A diethylenetriamine pentaacetic acid (DTPA) ligand core was appended with a bridging quinoline-type chromophore, which was further functionalised with a dipicolylamine unit (highlighted in red). For the Eu(III) complex, binding Zn(II) induced a 8.2-fold increase in quantum yield. The complex was then injected into HeLa cells and under normal levels of zinc showed no significant luminescence signal. However, upon addition of the zinc ionophore pyrithione and $ZnSO_4$ the cell

images brightened (Figure 14) suggesting that the Eu(III) complex bound to Zn(II).[36]

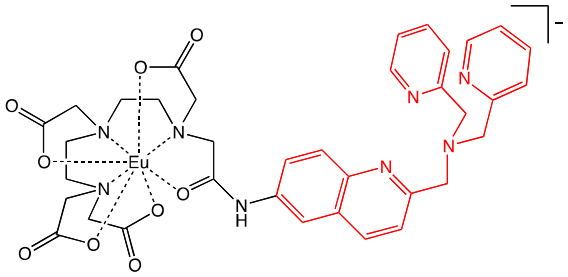

Figure 14. A Eu-DTPA derived complex (left) used as a zinc-responsive probe. The zinc binding site is indicated in red.

An emissive Eu(III) complex can probe and image singlet oxygen ($^1O_2$) over other reactive oxygen species. Derived from an aminocarboxylate-based 2,2′:6′,2′′-terpyridine ligand, which is substituted with a 9-anthryl unit (Figure 15), the complex is weakly luminescent. Reaction with $^1O_2$ converts the complex into a highly emissive species with long-lived luminescence. HeLa cells were co-incubated with the complex and a $^1O_2$ generating porphyrin photosensitiser and imaged using time-gated luminescence microscopy. Following irradiation, rapid evolution of Eu(III)-based luminescence was localized in the nuclei.[37]

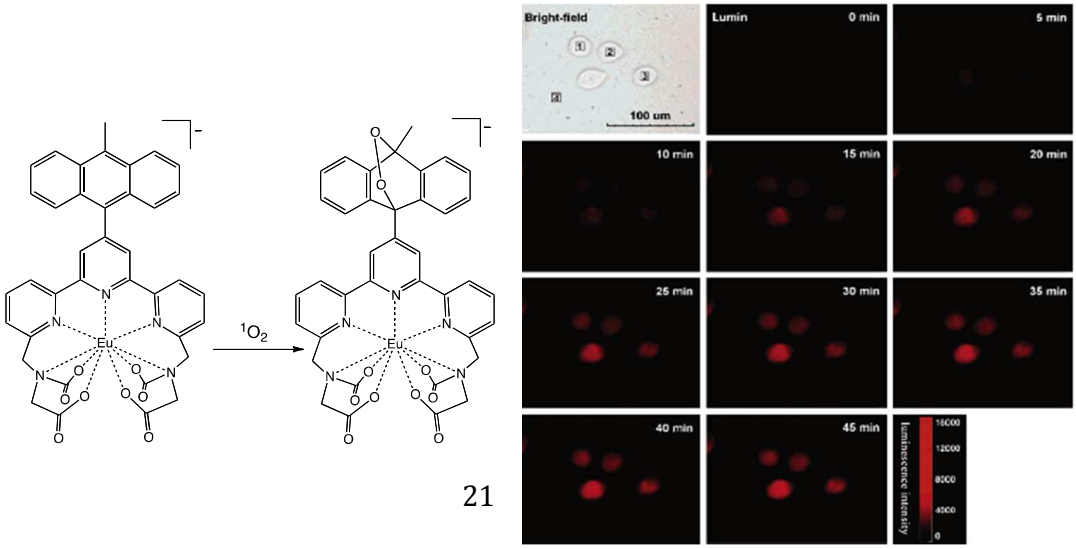

Figure 15. A $^1O_2$ reactive Eu(III) complex (left). Bright-field (regions 1-3 are the centre regions of three HeLa cells, and region 4 is an extracellular region) and time-gated luminescence images of the Eu-deposited HeLa cells at different irradiation times. Reprinted with permission from Song et al *J. Am. Chem. Soc*., 2006, **128**, 13442. Copyright 2006 American Chemical Society.

Parker and co-workers have previously reported[38] the use of sulfonyl amine groups as pH dependent donors to Ln(III), yielding pH-responsive luminescent and relaxometric probes. This method has now been applied to the TACN-derived ligands described above, whereby one of the pyridylalkynylaryl donors was replaced with *N*-methanesulfonylethylamine. Lifetime measurements on the Eu(III) complex revealed partial hydration (q > 0) at pH 4 and zero hydration (q = 0) at pH 9, whilst the modulated fine structure of the spectral profile was indicative of an alteration in the Eu(III) environment (Figure 16).[39]

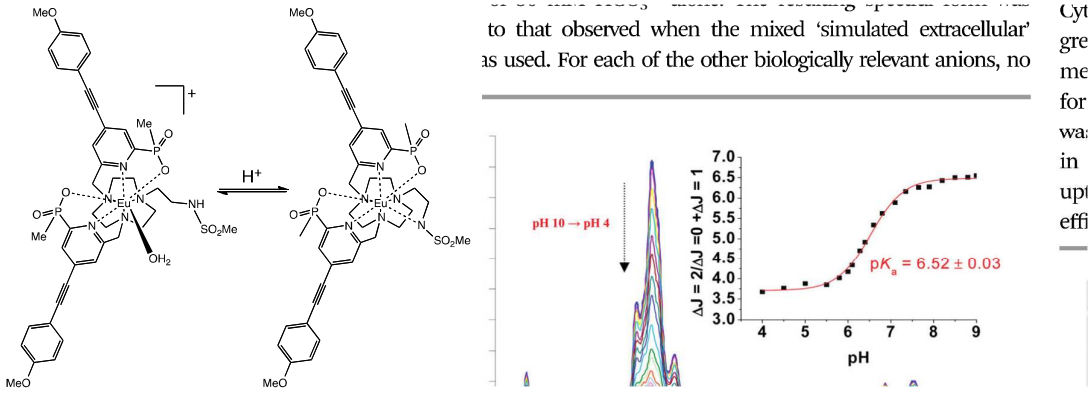

Figure 16. A Eu(III)-TACN complex showing pH-sensitive luminescence.

It is important to note that a number of research groups[40] have worked on the development of responsive luminescent probes based on Ln(III) complexes.

Some of the most promising systems[41] seek to modulate *q* (as shown above for the pH response) upon analyte binding. Such systems should be especially applicable to lifetime mapping microscopy (FLIM / PLIM), but have not been assessed under such conditions.

3. Magnetic Resonance Imaging and Contrast Agents

Magnetic resonance imaging (MRI) and computed tomography (CT) are the two most powerful radiological methods that are routinely used in the clinic. Both methods can provide finely detailed images, and with higher-field MRI becoming available, voxel resolutions of 100 μm are feasible. While standard hospital scanners (1.5 or 3 T) have a spatial resolution of about 1 mm and a time resolution of about a second, the current state of the art is the INUMAC imager.[42] Containing an 11.75T magnet and costing $270M, it will be able to image to 100 μm and see biological processes occurring per one-tenth of a second. While in theory this state-of-the-art instrument may be useful for the early detection of neurodegenerative disease, at the current cost it is hard to imagine its use on a world-wide stage, though one anticipates that technology will advance and costs of such magnets may diminish over time.

Technique	Resolution	Depth	Time	Sensitivity	Agents	Primary use
MRI	50-100μm	No limit	Min-hr	~10^{-6} M	Gd, Dy, Fe_nO_m	Versatile, high soft tissue contrast

CT	50μm	No limit	Min	~10^{-3} M	Iodine	Lung and bone
Ultrasound	50μm	cm	Min		Microbubbles	Vacular and interventional
PET	1-2 mm	No limit	Min	~10^{-12} M	^{18}F, ^{11}C, ^{15}O	Versatile
SPECT	1-2 mm	No limit	Min	~ 10^{-10} M	^{99m}Tc, ^{111}In	Labelled antibodies
Fluorescence microscopy	nm	mm	secs		fluorophores	Cell work

Table 3. Comparison of different imaging techniques.

MRI does not have the sensitivity of PET or SPECT, but it does have superior resolution (Table 3). However, the sensitivity (S/N) of MRI can be improved by the use of contrast agents (*e.g.* Figure 17) and from a chemist's view point, there is the added benefit that contrast agents may be designed to be responsive to their environment. With the possibility of switching the relaxation effects, SMART contrast agents are feasible. This is particularly attractive to the research chemist and allows higher S/N and hence sensitivity.

3.1 The Basic MRI Experiment

In essence, by placing a water molecule in a field gradient, the ^{1}H NMR resonant frequency of the protons in a water molecule is dependent upon the applied field. Thus, by placing a field gradient along the *x* then *y* and then *z*-axes, one is able to locate a water molecule in space. The true MRI experiment is a more complex situation, involving the spatial determination of all water molecules within the body, relying on the fact that water molecules in different parts of the body have different relaxation rates and hence differing signal intensities. In reality, the method requires significant data analysis, but the basic principles are the same as those familiar to NMR spectroscopy.

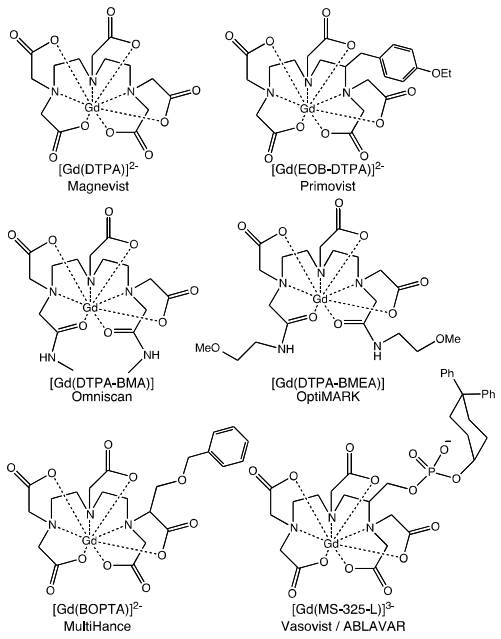

Figure 17. Examples of common commercially available MRI contrast agents.

The MR signal: Common Misconceptions in NMR and MRI

Due to a number of erroneous websites, many students think of the NMR signal as being due to the nucleus absorbing energy and nuclear spin moving from the *z*-axis to the –*z*-axis. This, of course, is not the case. It is better to think of the nucleus as a small spinning magnet, which in a magnetic field aligns on the *z*-axis, but if we irradiate it with a pulse of energy (a 90° degree pulse) the spinning magnet moves into the *xy* plane. Now imagine a magnet on a piece of string: if you spin it around and bring it close to a wire coil, the spinning magnet will induce a current in the coil. This is the basis of NMR and thus MRI.

Relaxation

Now, this spinning magnet in the *xy* plane does not stay there forever, and the signal is lost over time. Two main mechanisms cause a decay in the signal.

One is the T_1 relaxation, referred to as longitudinal or spin-lattice relaxation and it involves a return of the nuclear dipole from the *xy* plane to the *z*-axis. The other is T_2 relaxation, referred to as transverse or spin-spin relaxation. For this you must realise that, in the sample, all the nuclei spin (or precess) coherently in the *xy* plane. If this was not the case then there would be no net signal as it is the change in magnetic field that causes the signal and a totally random array of spins in the *xy* plane would result in no effective moment. The T_2 relaxation relates to a dephasing of the net magnetic moment in the *xy* plane. In simple terms, a short T_1 results in an increase in signal (as it allows us to rapidly apply 90° pulses to our sample) and a short T_2 results in a decrease in signal.

Contrast agents

In the MRI experiment, the difference in signal intensity for the different compartments of the body may be small. In such cases, the addition of a contrast agent, specifically localised to an area of interest, will increase image resolution and sensitivity.

Chemical reagents can affect T_1 and T_2 to varying degrees. If a reagent affects T_1 to greater extent it a T_1 or positive contrast agent which causes a stronger signal in its local vicinity, but if $T_2 > T_1$ then the opposite is true. While a number of different types of species have been reported as acting as effective contrast agents, such as paramagnetic *d*-metal ions Mn(II) and Fe(III) complexes, organic radicals, and metal oxide nanoparticles, this review will focus upon the use of molecular lanthanide complexes.

Positive Contrast agents

These species primarily affect the T_1 relaxation of solvent water molecules. Despite a few reports of the use of f^7 Eu(II) complexes, the overwhelming majority of T_1 molecular contrast agents are complexes of f^7 Gd(III). By understanding the theory relating to T_1 relaxivity and the prerequisites for *in vivo* use, the design of Gd(III) complexes will become clear, as will the current themes in the development of new reagents.

Relaxation Theory

The ability of a reagent to affect the T_1 of bulk water is expressed as its relaxivity (r_1). The r_1 of a complex is inversely related to the T_1 relaxation time for a solution of agent:

$$r_1(\text{obs}) = 1 / T_1(\text{obs}) \qquad [1]$$

but the observed T_1 has two components, one being the inherent relaxivity of the water solution and the other component due to the interaction between water molecules and the contrast agent. There is a linear relationship between contrast agent concentration and this component to relaxivity:

$$r_1(\text{obs}) = 1 / T_1\,(\text{diamagnetic}) + r_1\,[\text{Gd}] \qquad [2]$$

Hence, r_1 may be determined by measuring r_1(obs) for varying concentrations of contrast agent. A plot of r_1(obs) *versus* [Gd] will have a gradient of r_1. Conventionally, the concentration is expressed as mM and hence the units of relaxivity are $mM^{-1}s^{-1}$. The value is both field and temperature dependent and these parameters must be stated when r_1 is reported. This value of r_1 may be further segregated into its components:

$$r_1 = \quad r_1^{IS} + r_1^{OS} + r_1^{SS} \qquad [3]$$

where r_1^{IS} is the inner sphere relaxivity due to the interaction between Gd(III) and water protons in the first coordination sphere (the effect is transmitted to the bulk solution *via* chemical exchange of the inner sphere protons); r_1^{OS} is the outer sphere relaxivity due to the bulk solvent molecules diffusing around the paramagnetic centre experiencing a paramagnetic effect (relaxation due to the random translation diffusion is outer sphere relaxation); r_1^{SS} is second sphere relaxivity. Water may also hydrogen bond to the ligand or the inner sphere water and in theory, it may be treated the same as inner sphere relaxation. Separation of inner and outer sphere relaxation is based on the intra- and intermolecular nature of the interaction. In addition, it is difficult to separate and evaluate the magnitude of second sphere relaxation as it *appears* as an increase in outer sphere relaxation.

Typically for Gd(III) complexes $r_1^{IS} \approx r_1^{OS}$, and while some work has focused on the variation of r_1^{SS},[43] most efforts aimed at modifying or increasing r_1 involve the variation of r_1^{IS}.

The inner sphere relaxivity is expressed by the equation:

$$r_1^{IS} = [cq/ 55.5] . [1/ T_{1m} + \tau_m] \qquad [4]$$

here, c = conc of gadolinium; q = number of bound water molecules; 55.5 is the concentration of water; T_{1m} is longitudinal proton relaxation rate of bound water; τ_m = lifetime or residence time of inner sphere solvent.

On reflection, it can be seen from Eq. 4 that the first term is the mole fraction of water bound to the gadolinium, while the second term relates to the ability of the complex to relax the bound water molecules and propagate this effect to the bulk solution. The relaxation of bound water (T_{1m}) is governed by magnetic field dependent dipole-dipole (DD) and scalar/contact mechanisms (SC) and for longitudinal relaxation SC mechanisms provide a negligible contribution. Solomon-Bloembergen-Morgan theory allows us to identify important parameters that affect T_{1m} and hence r_1. DD interactions are modulated by the reorientation of the nuclear spin-electron spin vector, electron spin relaxation and the water/proton exchange rate.

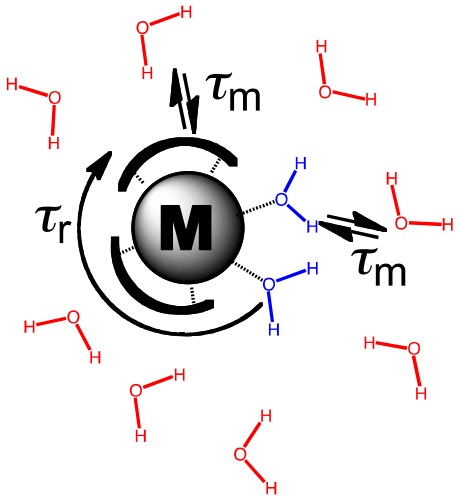

Scheme 3. Cartoon representation of important parameters of a q = 2 complex that influence relaxivity.

3.2 Optimising relaxivity

From this, we can see that for the optimisation of relaxivity (r_1) we can target: (i) the q number; (ii) rotational correlation time, τ_r ; (iii) the water exchange

rate; (iv) *S* (total spin quantum number) and T_{1e} (spin-lattice electronic relaxation time); (v) second sphere relaxivity. Each of these factors is discussed separately below.

(i) The *q* number

As discussed earlier in the context of lanthanide luminescence, the *q* number can fundamentally influence the physical properties of the complex (Scheme 3). From equation 4, it can be seen that this is the number of water molecules coordinated to the lanthanide centre and that the observed relaxivity is linearly proportional to *q*. However, in practice, we cannot and do not simply increase *q* to obtain maximal relaxivity. There are several reasons, discussed below, why this is not practical, desirable or optimal.

Toxicity of 'free Gd(III)'

$GdCl_3$ is toxic with an LD50 of 100-200mg/kg and it is deposited in the liver, bones and lymph system. However, by chelating a ligand to the metal, the toxicity of the imaging agent may decrease >100 fold. However, the variation of toxicity between contrast agents varies greatly with the thermodynamic stability and/or kinetic inertness of the complexes. That is, if a metal is (i) firmly attached to the ligand (thermodynamic stability) or the metal is very slow at dissociating from the ligand (kinetic inertness), then one expects this complex will be less toxic. Thus, $[Gd(H_2O)_8]^{3+}$ may have a moderately high relaxivity, but it would be toxic at the concentrations utilised in the clinic. Therefore a range of ligands has been developed by chemists for the encapsulation of lanthanide ions for use in luminescence, PET and MRI applications (some of which were discussed earlier). Clinically utilised

reagents are typically derived from two families of ligands: acyclic, polydentate ligands based upon the DTPA framework which possess high thermodynamic stability, or cyclic polydentate ligands based upon a DOTA framework (Figure 18) which possess both high thermodynamic stability and high kinetic inertness. However, to obtain this high stability, the ligands are often seven or eight coordinate meaning that *q* will be 2 or 1. Often, in designing a new ligand, one anticipates that the higher the value of *q*, the lower the stability may be. Thus the design of a new ligand is a careful balancing act of trying to lower ligand denticity, while trying to retain or improve the stability of the complex. Even once a new complex has been identified, there is still a possibility that when the complex is placed in biological media a ternary complex may form, with for example, a phosphate ion replacing bound water molecules and so reducing *q* and the observed relaxivity.

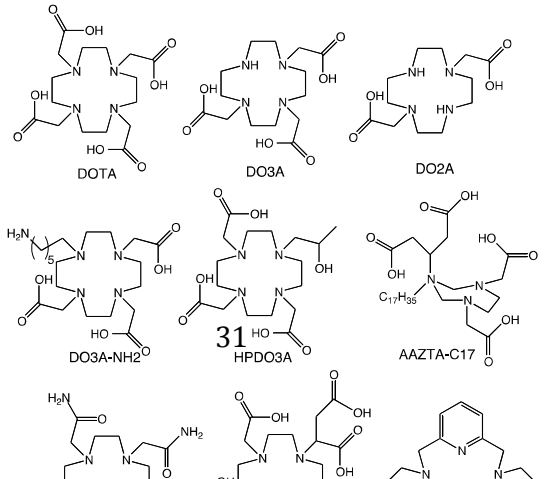

Figure 18. Selection of common macrocyclic ligands for Gd(III).

Clinically Utilised Ligands, q values and stability constants

It is somewhat surprising that the majority of the clinically utilised ligands are based upon the DTPA ligand framework (Figure 19), with DOTA and its related compounds being used to a lesser degree. For example in 2007, only ~18% of the MRI contrast agents used were based on macrocyclic cyclen ligands, with Bracco's Prohance being utilised more than Guerbet's Dotarem®. The most used contrast agent was Magnevist (Bayer Schering Pharma), with ~51% followed by Omniscan (~25%, GE Healthcare).[44] The thermodynamic stability of these compounds can be measured, by competitive acid-base titrations, and the value is expressed as the log *K* (see Table 4).[45]

	Cases of NSF	CAs Admin. (Millions)	% of the market	Incident/ Million doses	Stability (log *K*)	Dissoc. half-life
Omniscan	438	47	25.23	9.3	16.8	30 sec
OptiMARK	7	0.8	0.43	8.8	16.8	
Magnevist	135	95	50.99	1.4	22.2	10 min
MultiHance	0	6	3.22	0	22.6	
Primovist	0	0.15	0.08	0		
Vasovist	0	0.05	0.03	0		
Gadovist	1	2.6	1.40	0.4		
ProHance	1	12.3	6.60	0.1	23.8	3 hr
Dotarem	1	22.4	12.02	0	25.6	338 hr
Total	583	186.3	100	-	-	-

Table 4. General properties of commercially available MRI contrast agents.

Nephrogenic Systemic Fibrosis

First observed in 1997 and formally recognised in 2006, over time there have been increasing numbers of reports detailing the toxic effects of Gd(III)-based contrast agents in patients who have impaired kidney function. Nephrogenic Systemic fibrosis (NSF) results in fibrosis of skin, joints, eyes, and internal organs, the condition may result in fractured bones or even death. It is considered that the release of free Gd(III) from the contrast agent is the root cause of NSF and Table 3 shows how the complexes with low stability constants have the highest incident of NSF. However, when comparing Magnevist to Dotarem, both have significant thermodynamic stability and it is the kinetic inertness of the latter which is seemingly beneficial. Currently, Omniscan and Optimark are considered to carry the greatest risk, followed by Magnevist and Multihance while Dotarem (using DOTA) and Prohance (using HPDO3A) are considered the less likely to release Gd.

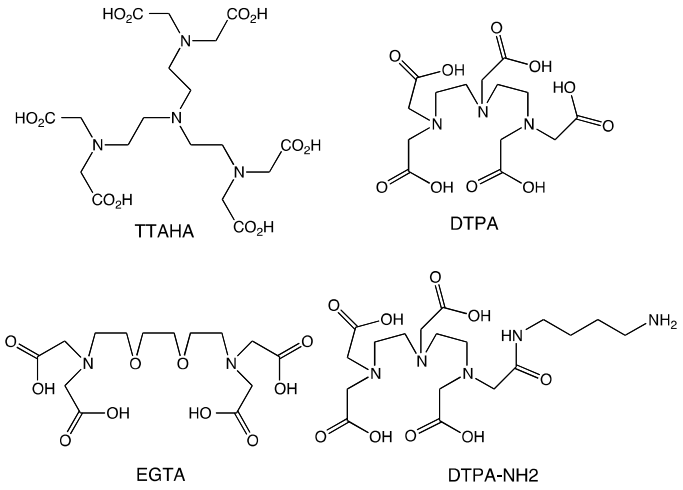

Figure 19. Example of acyclic ligands for Gd(III).

Ternary Complexes

It is generally recognised that a high *q* number will result in a higher relaxivity. But even if one designs a new ligand resulting in a stable/inert complex with a low denticity, the resulting complex may still have a low *q* number. This is due to the formation of ternary complexes where a secondary ligand complexes to the metal centre displacing solvent water molecules. This is particularly problematic for cationic complexes which readily bind carboxylate and/or phosphate ions and was discussed earlier in the context of luminescence (Scheme 2). One approach is to develop ligands that give anionic Ln(III) complexes: the overall negative charge will electrostatically repel other anions in solution.

Cage structures incorporating Gd(III)

An ingenious approach to solving the problem of having a high *q* value without the toxicity, involves trapping the Gd(III) within a cage on the molecular scale.

The use of buckminsterfullerenes to surround the metal ion has proved successful, but the parent fullerenes required derivatisation to yield water soluble products. High relaxivities have been observed for alcohol derivatised fullerenes (r_1: $Gd@C_{82}(OH)$ is 67 $mM^{-1}s^{-1}$ (298K, 20 MHz, pH 7.5), about 40 times greater than that of Magnevist,[46] but the molecules do suffer from significant reticuloendothelial system (RES) uptake. However, carboxylate functionalised analogues, although having a lower relaxivity,[47] do not suffer from this problem. It remains to be seen if the synthesis of such molecules could ever be carried out on a commercial scale, suitable for the pharmaceutical industry.

(ii) The rotational correlation time, τ_r

Molecular motion causes local changes in the magnetic field and this has a significant effect in changing the rate of relaxation. As described by SBM theory, proton relaxivity of small low molecular weight contrast agents may be limited by fast rotation and low hence low τ_r values (τ_r is the time taken to reorientate and high values indicate slow movement). This has prompted the development of new agents to slow down rotation and thus increase r_1.

Polymeric and Dendrimeric Structures

The Stokes-Einstein equation predicts τ_r to be proportional to r^3 (where r is the effective radius of the molecule). Thus, the attachment of small molecule contrast agent, based on DTPA or DO3A, to a macromolecular species will produce large species with long reorientation times. There are legions of polymers which have been utilised with this aim, but a key consideration

would be the biocompatibility of the polymer. An example is the formation of DTPA-polyethyleneglycol species, with the two moieties conjoined by an amide link. Magnevist and Omniscan (Figure 17) have τ_r values of 58 and 66 ps respectively, but upon the formation of the polymer (MWt 20.2 kDa) there is a modest increase in τ_r to 232 ps[48], resulting in modest changes to r_1 (6.31 $mM^{-1}s^{-1}$, 20 MHz, 310K; compared to 4.02 and 3.96 $mM^{-1}s^{-1}$ for Magnevist and Omniscan under similar conditions). An alternative ploy was the attachment of the contrast agent to a dendrimer, the advantage being that the dendrimer would have a well defined structure with a precise number of Gd(III) chelates attached at the periphery of the macromolecule. For example, the 3rd, 4th and 5th generation dendrimers possess 24, 48 and 96 surface reactive groups allowing 23, 30 or 52 Gd(III) complexes to be attached. The resulting dendimers have τ_r values of 580, 700 and 870 ps, respectively. While the resulting relaxivities are increased (14.6, 15.9 and 18.7 $mM^{-1}s^{-1}$, 20MHz, 310K),[49] the values are still somewhat lower than one might expect. It was recognised that the nature of the chelate linker can allow rapid movement of the contrast agent: the slow rotational dynamics of the macromolecule are not transduced to the local Gd(III) chelates. Therefore it is important to consider the nature of the linker units and the rigidification of the Gd(III) chelate.[50]

Micelles and Liposomes

As an alternative to covalently conjugating the contrast agent to a polymer, the association of a surfactant contrast agent to a micelle or liposome has also been explored. Hovland prepared an amphiphilic Gd-PCTA-[12]

derivative which formed micelles in aqueous solution.[51] With a relatively low critical micelle concentration (0.15 mM, 298K), r_1 is concentration dependent with a maximum relaxivity (29.2 $mM^{-1}s^{-1}$, 20 MHz, 298K) occurring at 1mM with micelle formation. The high relaxivity is a consequence of not only a long τ_r, but also a favourable water residence time.

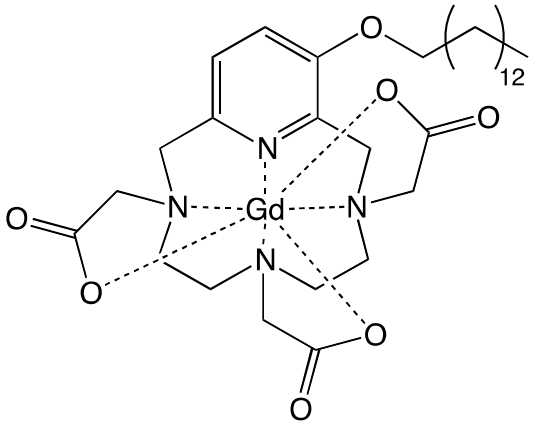

Figure 20. A lipophilic Gd(III)-PCTA derivative.

Similarly, Hovland also made highly lipophilic Gd(III) complexes for liposome incorporation (Figure 20).[52] Using liposomes composed of cholesterol and phospholipids with short acyl chain lengths (DMPC and DMPG), the loading of Gd-chelate and the amount of cholesterol in the liposomes were varied and the relaxivity studied. The highest relaxivity (52 $mM^{-1}s^{-1}$, 20 MHz) was found in liposomes with no cholesterol and a low content of Gd-chelate.

Related to this, a low-density lipoprotein (LDL) particle was functionalized with a Gd-DO3A-monoamide chelate with a long alkenyl anchor. Intercalation into the lipid layer of the LDL particles led to a significant enhancement of the MRI signal of atheroplaques in atherosclerosis mouse models.[53]

Clearly, the interaction between the amphiphilic ligand and macromolecule in these examples is non-covalent and weak. One drawback of such species is that they will not exist at low concentrations and, in addition, the possible redistribution of the contrast agent to other structures when placed in the body cannot be ignored. In an attempt to form macromolecular contrast agents which are more stable, Wang carried out the mini-emulsion polymerization of a monomer along with amphiphilic Gd(III) metallosurfactants. Using DO3A or DTPA-based complexes, particles with a 20 or 48 nm diameter were formed (the structures were stable to a dilution to 0.02mM) giving relaxivity enhancements of 11.1 $mM^{-1}s^{-1}$ (from 4.3 $mM^{-1}s^{-1}$) and 6.7 $mM^{-1}s^{-1}$ (from 4.5 $mM^{-1}s^{-1}$) for the respective reagents. The relaxivities were measured at 3T (129 MHz), but no temperature was reported.[54]

Binding to receptors and surfaces

Perhaps one of the earliest and most impressive examples of how relaxivity can be increased upon lengthening τ_r was the increase observed when lipophilic Gd(III) complexes bound to blood protein. Aime has expanded upon his earlier work and recently reported a lipophilic Gd(III) chelate with a long aliphatic chain (Gd-AAZTAC17; q = 2, τ_m = 67 ns), with a relaxivity of 10.2 $mM^{-1}\,s^{-1}$; at concentrations greater than 0.1 mM, the complex forms micelles (5.5 nm) with a relaxivity of ~30 $mM^{-1}\,s^{-1}$ (20 MHz and 298K).[55] Gd-AAZTAC17 (Figure 18) also exhibits good affinity for human serum albumin (HSA); the relaxivity shown by Gd-AAZTAC17/defatted HSA was 84 $mM^{-1}\,s^{-1}$ (20 MHz, 298K) is among the highest reported for a non-covalent paramagnetic adduct with a slow-moving substrate.

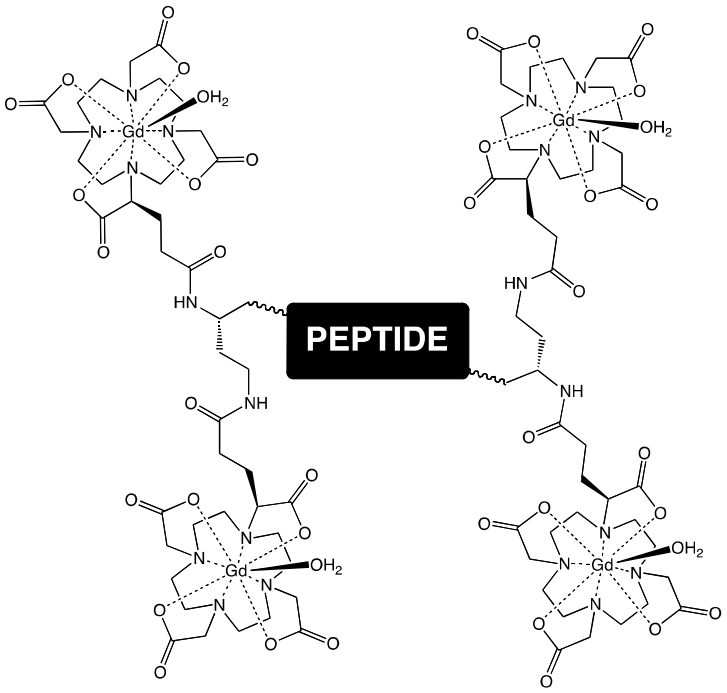

Figure 21. Abbreviated structure of EP-2104.

There are many other examples of restraining and attaching small Gd(III) complexes to large macromolecules, and these may be biological macromolecules (*e.g.* apoferritin), spore capsules and viral capsid or non-biological (*e.g.* gold nanoparticles or iron oxide nanoparticles). A recent example which serves as a thorough investigation of how slow tumbling of the Gd(III) centre affects relaxivity, is a study of the binding of gadolinium complexes (compared to gadolinium ions) to a graphene oxide surface.[56] The study indicates significant relaxivities for a Gd-DO3A-NH2 (Figure 18) complex when associated with the graphene oxide surface (r_1 = ~65 $mM^{-1}s^{-1}$, ~40MHz), the value was approximately twice that of analogous Gd-DTPA-NH2 species (Figure 19) and reflected the different *q* values in the two

complexes (Gd-DO3A-NH2, q = 2; Gd-DTPA-NH2, q = 1). The study also emphasises the power of supporting nuclear magnetic resonance dispersion (NMRD) measurements: calculated parameters (including τ_m and τ_r) can be obtained by fitting the variation in relaxation rate with varying applied magnetic field.

We have already seen the example of Gd-AAZTAC17, a lipophilic molecule designed to interact with HSA and in doing so lengthen τ_r and significantly enhance the relaxivity. Perhaps the best example is the ligand MS325 developed by EPIX, who were liquidated in 2010 (once sold as Vasovist, it is now marketed as ABLAVAR by Lantheus Medical Imaging; Figure 17). MS-325 (Figure 17) is a novel blood pool contrast agent to assess blockages in arteries. By strongly binding to HSA, the plasma half-life is lengthened, and r_1 is increased in due to a 60-100-fold increase in τ_r (10.1 +/- 2.6 ns *vs* 115 ps free) upon binding.

Another example of protein binding, also developed by EPIX, is the contrast agent EP-2104R (Figure 21). It is an MRI contrast agent designed to detect blood clots by binding to the protein fibrin, present in all thrombi.[57] EP-2104R comprises an 11 amino acid peptide derivatised with two Gd-DOTA-like moieties at both the C- and N-termini of the peptide. EP-2104R binds equally to two sites on human fibrin (K_d = 1.7 ± 0.5 μM) and has excellent specificity for fibrin over fibrinogen (over 100-fold) and for fibrin over serum albumin (over 1000-fold). The relaxivity of EP-2104R bound to fibrin was 17.4 $mM^{-1}s^{-1}$ (310K and 60MHz). Strong fibrin binding, fibrin selectivity, and high molecular relaxivity enable EP-2104R to detect blood clots *in vivo*.

(iii) Water-exchange rates[58]

As shown in equation 4, the rate at which water molecules bound to the Gd centre are exchanged with the bulk water is also of importance, as it is this exchange process (of water or protons) which allows the bulk to relax, not just those attached to the metal centre. In fact, there are many examples where τ_r has been optimised, but the gain in relaxivity is limited due to slow water exchange. Accordingly, significant work has sort to gain an understanding of the exchange process and determine how to control its rate. The mechanism by which this process occurs may be dissociative or associative, depending on the nature of the complex and the mechanism may be determined by measuring the volume of activation (a positive volume indicating a dissociative process). Simplifying the situation, an associative process will require a sterically non-demanding ligand, which will allow the metal to expand its coordination sphere, while rigid ligands yielding complexes with low *q* values will favour a dissociative process; Table 5 lists a variety of well known complexes and gives their mechanism if known. The rate of the process may be measured by studying the temperature dependent ^{17}O NMR of aqueous solutions of these complexes.

Complex ligand	*q*	K_{ex}^{298} ($\times 10^6$ s^{-1})	Mechanism
aqua	8	804	A
DTPA	1	3.30	D
DTPA-NMA	1	1.3-1.9	D
DTPA-BMA	1	0.45	D
DOTA	1	4.1	D
DO3A	1.9	11	
DO2A	2.8	10	
DOTASA	1	6.3	
TTAHA	2	8.6	D
PCTP-[12]	1	170	I_a

Table 5. Water exchange parameters for common Gd(III) complexes.

There are several points to note. It is the rigidity of the inner sphere coordination that is important and it is changes to the inner sphere that result in changes to the exchange rate. Compared to the aqua species, all Gd(III) amino carboxylates have much lower rates of exchange. Nearly all complexes go from 9 to 8 coordinate and this requires a high activation energy. The rigidity of the inner sphere plays an important role: replacing a carboxylate for an amide decreases the rate by a factor of 3-4 (*e.g.* DTPA *vs* DTPA-NMA *vs* DTPA-BMA). This may be explained by steric crowding, as the amide is *less* crowded, due to the longer Gd-O bonds. The steric crowding of the ligand pushes water away from the metal centre, easing the dissociation step. Exchange rates are hardly affected if substituent changes do not affect the inner coordination sphere. The charge on the complex is also important, with negatively charged complexes again facilitating the dissociative process. Accordingly DOTASA yields a complex with a 50% higher exchange rate compared to DOTA. In addition, the TTAHA complex has two water molecules, decreasing the inner sphere rigidity, and so increasing the exchange rate relative to the DTPA complex. However, the similar relaxivities of Gd-DO2A and Gd-DO3A, despite the lower inner sphere rigidity, may be ascribed to the adverse effect of the increased positive charge in the Gd-DO2A complex. Finally, with the exception of a few protein bound complexes, the inclusion of a monomeric Gd(III) chelate into a macromolecular/polymeric structure does not significantly affect water exchange kinetics.

Finally, it is worth noting that while there is a general movement towards longer τ_r values and shorter water exchange rates, it should be remembered that there is a subtle interplay between these two parameters

which requires some attention. Desreux has highlighted this point, showing that, with a low τ_r, the observed modest relaxivities do not change greatly if the water exchange rate changes (from one metal complex to another).[59] But, when τ_r is much higher, the relaxivity is much more sensitive to the water exchange rate, and values which are both too high or too low are detrimental to the observed relaxivity.

(iv) *S* and T_{1e}

By definition, it is impossible to modify *S* if we are utilising Gd(III). Furthermore, for a mononuclear complex, *S* is optimal for Gd(III) and it is beneficial in having a long T_{1e} which allows an effective interaction between the relaxing electron of the metal ion and the relaxing nuclear spin of the proton. For a detailed discussion of the interaction of such spin systems, Lucinat has reviewed these interactions for a wide variety of metal ions.[60]

While it is difficult to imagine how we may design modifications of T_{1e} in Gd(III) complexes, it is worth noting that the Gd-AAZTAC17 complex mentioned above, forms micelles (5.5 nm) at concentrations greater than 0.1mM, with a relaxivity of ~30 $mM^{-1} s^{-1}$ (20 MHz and 298K). A relaxivity of 41 $mM^{-1} s^{-1}$ was recorded when 98 % of the Gd(III) ions were replaced by diamagnetic Y(III). In other words, the relaxivity is "quenched" by magnetic interactions between the Gd(III) ions on the surface of the micelle, causing a decrease in the electronic relaxation time.

Second-sphere Relaxivity[38]

Water associated with the contrast agent may be defined as inner sphere (directly coordinated to the metal) or outer-sphere (water molecules diffusing

past the complex). The outer-sphere may often contribute 40-50% of the total relaxivity and largely depends on the distance of closest approach. Typically this does not vary too much for most compounds. However, there is an additional consideration to be made: some water molecules may be held close to the complex for longer than might be expected (longer than the diffusional correlation time) due to hydrogen bonding interactions with functional groups on the ligand. In such cases, the behaviour of these water molecules is described in the same way as an inner-sphere water molecule and it is difficult to discriminate the two.

However, by careful choice of complex, *e.g.* complexes with $q = 0$, it is possible to separate outer-sphere relaxivity from second sphere relaxivity. Aime *et al* have carefully studied relevant complexes and in one example were able to show that a relaxivity enhancement upon binding with a protein was due to a number of second-sphere water molecules held about the Gd(III) centre.[61]

3.3 Responsive contrast agents

As discussed earlier in the context of luminescent lanthanide complexes, an ability to report on the (biological) environment is highly desirable for *in vivo* imaging. With an understanding of how the relaxivity of a contrast agent may be modified or optimised, it is then possible to design responsive agents which can potentially allow *in vivo* imaging of chemical species or biological processes. While such 'smart' devices are yet to be used in the clinic, a number of compounds have been successfully used in research and it is an avenue of contrast agent design which is understandably receiving much

interest. Again, the following examples are in no way comprehensive, but they aim to give the reader an insight into how the appropriate ligand design can yield smart devices.

Enzyme Responsive

An early example of an enzyme responsive agent was prepared by Anelli et al.[62] A novel Gd-DTPA derivative (Figure. 22) with a built-in sulfonamide (SA) was synthesized to selectively target the enzyme carbonic anhydrase. The longitudinal relaxation rates of aqueous solutions of Gd-DTPA-SA in the presence of carbonic anhydrase increased significantly. The complex interacts with erythrocytes, presumably due to a high affinity for the carbonic anhydrase present on their outer surface. The interaction of Gd-DTPA-SA with serum proteins was negligibly small so the complex may potentially be tested as a selective contrast agent for compartments outside the blood pool.

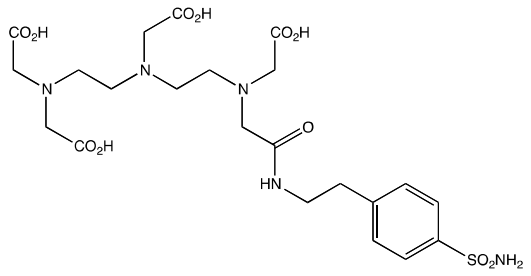

Figure 22. Molecular structure of DTPA-SA.

Another example of enzyme responsive agents is Meade's galactosidase-reactive complex. In this DO3A derivative, the ligand has a pendant galactopyranose group, which, when cleaved in the presence of galactosidase increases the *q* number of the complex. Beta-galactosidase is a commonly

used marker gene, and thus regions of higher intensity in the MR image correlate with regions expressing marker enzyme. The contrast agent offers promise of *in vivo* mapping of gene expression in transgenic animals and offers a general approach for constructing a family of MRI contrast agents which can respond to biological activity.[63]

An alternative approach to measuring galactosidase expression was taken by Aime. In this approach, the contrast agent contains a galactose protected tyrosine group. Galactosidase produces a tyrosine group, which, in the presence of tyrosinase, yields a polymeric product with an accompanying increase in r_1.[64]

pH Responsive

There are many examples of pH-responsive contrast agents and often they are based upon the protonation and deprotonation of bound water ligands which perturb the water exchange rates, or the protonation/deprotonation of pendant amino/amido/alcohol groups which then modulate the *q* value. In addition, the protonation/deprotonation of polymer-based Gd(III) agents will adjust the polymeric structure and modify any observed relaxivity. For example, a 114-residue polyornithine with 30 attached Gd-DO3A moieties and 84 pendant amines. In acid conditions, the amine groups are protonated and the structure is stretched out and flexible, but in basic conditions, the polymer shrinks and is more rigid: these changes in structure cause a 40% variation in the observed r_1.[65]

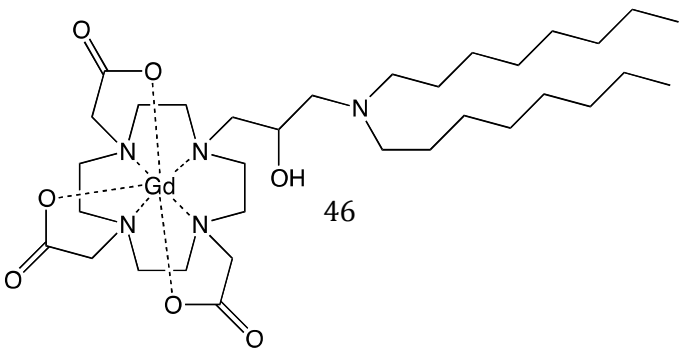

Figure 23. Molecular structure of Gd-HADO-DO3A.

Similarly, Hovland has prepared a series of Gd-DO3A derivatives which mimic phospholipids. Two complexes were evaluated as pH responsive MRI contrast agents *in vitro*. The T_1 relaxivity (r_1) of Gd-HADO-DO3A (Figure. 23) increased by 142% (to 18 $mM^{-1}s^{-1}$, 10 MHz, 298K) as the pH changed from 6 to 8. The pH dependence arises from the formation of supramolecular structures caused by deprotonation of the amphiphilic complex at alkaline pH.[66]

Metal Ion Responsive Agents

There are increasing numbers of reports of contrast agents which can selectively detect the presence of metal ions. The design of these complexes is often analogous to the related luminescent sensors (indeed luminescent lifetime measurements on Eu(III) analogues are frequently used to support relaxivity data on Gd(III) species),[67] with the binding of the metal ion often modifying the *q* value of the Gd(III) centre. There has been particular interest in synthesising complexes which can detect biologically important analytes such as Zn(II), Cu(II), Fe(II) and Ca(II). Some examples of ligand design include a DTPA-BMA (Omniscan) derivative where the two ethylamide groups are replaced with 2,2′-dipicolylamine groups (Figure. 24).[68] On addition of

Zn(II) to the Gd(III) complex, the two dipicolylamine moieties come together to coordinate the Zn(II) molecule and in doing so hinder the access of water molecules to the Gd(III) centre. A reduction in relaxivity from 6.06 to 3.98 mM^{-1} s^{-1} (300 MHz, 298K) was observed when one equivalent of Zn(II) was added. No reduction in relaxivity was observed when Mg(II) or Ca(II) was added.

A final example of Zn(II) detection utilises a DO3A ligand with a pendant iminodiacetate group (Figure. 24).[69] In the absence of Zn(II), the acetates bind to the Gd(III) centre and restrict water access resulting in a low relaxivity (2.33 $mM^{-1}s^{-1}$, 60 MHz). On addition of Zn(II) the relaxivity increases to 5.07 $mM^{-1}s^{-1}$, consistent with one water molecule bound to Gd(III) (q = 1). Using this system, Zn(II) concentrations as low as 100 μM can be detected. No observed change in relaxivity was observed when either Ca(II) or Mg(II) were added. Interestingly, a similar ligand has been reported for the selective imaging of Cu(II).[70] While it was stated that Zn(II) gave no enhancement of relaxivity, the experiment was run in phosphate buffered saline (PBS) and it is likely that the formation of insoluble zinc phosphate forms preferentially to the Gd-Zn adduct.

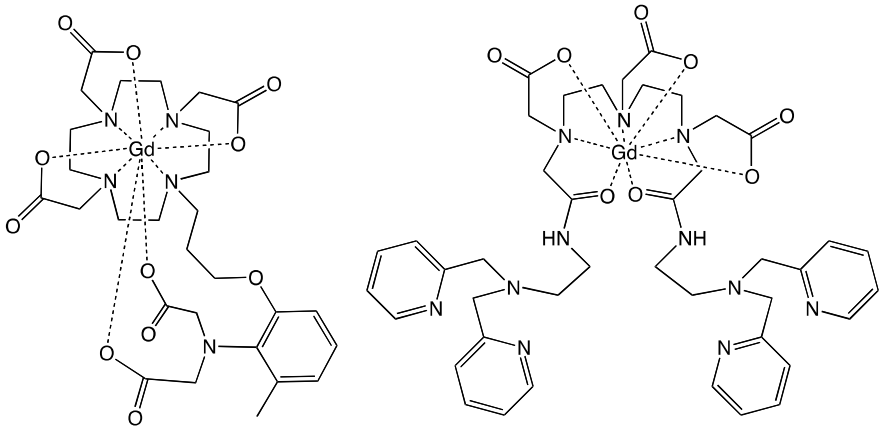

Figure 24. Metal ion responsive Gd(III) agents.

4. CEST and PARACEST[71]

A more recent addition to the field of MRI contrast agents is that of chemical exchange saturation transfer (CEST) agents. Building upon the original work of Ward *et al*, [72] a series of paramagnetic CEST agents have been synthesised and many of these agents contain a lanthanide centre.

The basic approach may be understood by considering the fact that upon irradiating a given peak we will saturate its resonance, leading to a reduction in the signal. A CEST agent is a species with a labile proton, exchanging with bulk water. If the proton exchange rate is smaller than the separation of the two proton resonances, then the saturation of the CEST proton may be transferred to the bulk solution resulting in a depression of the bulk water signal. The rate of this exchange is important: naturally, we wish it to be as fast as possible, to enhance the exchange effect, but the process must remain in the slow-intermediate exchange rate domain to ensure that two discrete resonances (bulk water and agent) are observed by NMR.

The slow-intermediate exchange rate is defined as: $\Delta\omega_{CA}/k_{CA} >> 1$ where $\Delta\omega_{CA}$ is the chemical shift difference (in rad/s) between the exchange site proton and water, and k_{CA} is the rate of exchange.

Unfortunately, when imaging the experiment cannot be quite so simple, as upon irradiation, a depression of the signal may be observed even without the CEST agent (due to the broad signal of proton in a biological matrix). To circumvent this problem, a secondary experiment is run, but this time irradiating at the same distance form the water peak, but in the opposite

direction. While a reduction in the water signal may be observed, it will be of a lesser magnitude to the first experiment. Now the saturation transfer (ST%) may be expressed as $100 \times (1 - \text{Intensity}_{\text{on-resonance}}/\text{Intensity}_{\text{off-resonance}})$. The CEST agent's effectiveness is not measured by relaxivity, but instead can be measured by ST% compared to the agent concentration.

These basic ideas have been greatly extended and have allowed a generation of new agents, namely PARACEST[73] and LIPOCEST. A series of lanthanide complexes have been prepared and varying exchanging protons, have been investigated. These may be protons on waters bound to the metal centre, or they may be exchangeable protons on the ligand. Notable examples are the exchangeable –NH- peaks, which may be designed into a DTPA or DOTA type ligands *via* amide-type linkages. Furthermore, Aime[74] has utilised complexes with two exchangeable protons (slowly exchanging water and N*H* on a ligand) to ratiometrically image pH (the two proton exchange rates differ in their response to pH). Obviously, these PARACEST agents are different to standard Gd(III) contrast agents, as they cause a dark image contrast, but there is significant interest in developing these agents as they offer the possibility of enhanced sensitivity. Sherry has recently comprehensively reviewed the subject of PARACEST agents.[75]

Finally, LIPOCEST agents[76] are nanoparticular systems with extremely high numbers of mobile protons and so offer high contrast. More precisely, these are liposomes with hydrophilic lanthanide complexes, typically based on Dy(III) or Tm(III), trapped in the liposomal compartment. With up to 10^9 mobile protons within the liposome, these reagents may show great sensitivity (< 100 pM).

5. Multimodal Imaging

As mentioned earlier, a number of imaging techniques are available at a biomedical level with various pros and cons associated with each (Table 5). Therefore combining two or more imaging modalities into a single molecule can circumvent many limitations associated with a particular technique, whilst simplifying aspects of the agent administration and biodistribution characteristics (pharmacodynamics). The reader is directed to some recent excellent reviews that provide further details on a range of interesting examples, some of which include Ln(III) systems.[77,78,79,80] Brief descriptions of examples incorporating lanthanide ions are highlighted below.

MR/optical probes

In essence a large number of chromophore appended Gd(III) complexes, which are synthesised as analogues of Eu(III) species, have the potential to deliver both MR and optical imaging capability.[81] However, the residual fluorescence characteristics of the chromophore are often non-ideal for biological applications. A simple approach is to covalently link common biocompatible organic fluorophores (*e.g.* fluorescein or bodipy[82]) to DOTA-type, or similar, Gd(III) chelates: a large number of putative dual modal MR/optical imaging agents have been reported using such an approach. Long and co-workers have reported rhodamine functionalised Gd(III) complexes based on a DOTA framework.[83] The compound shown in Figure 25 is water soluble (aided by the amide functionality), has r_1 = 3.84 $mM^{-1}s^{-1}$ (9.4 T, 298K), and shows pH-sensitive, rhodamine-centred fluorescence. The probe was cell

penetrating and localised in the mitochondria of HEK (human embryonic kidney) cells, whilst imaging with 4.7 T MRI was obtained on nude mice with xenografted tumour implants.

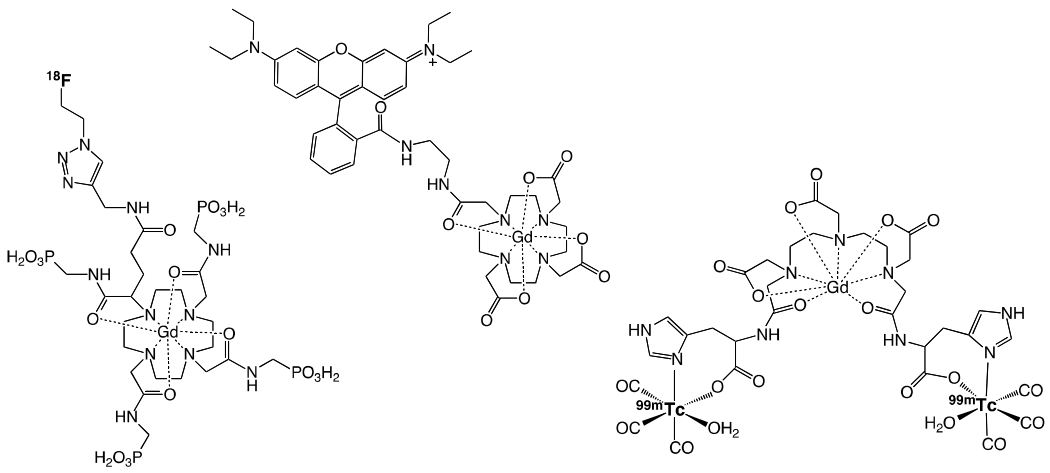

Figure 25. Examples of multimodal agents that contain Gd(III).

MR/radionuclide probes

A number of innovative systems have been described that combine radionuclides with Gd(III) chelates. The common challenge is the time-limiting synthesis and purification associated with the isotope labelling step, which should be completed within 3 × $t_{½}$ (half-life) for the chosen radionuclide (for ^{18}F, $t_{½}$ is 109.8 min); 'Click Chemistry' is a popular means for adding radiolabels quickly and efficiently. Figure 25 shows an example of such an approach that couples ^{18}F with a traditional Gd(III) macrocyclic chelate to give a MR/PET probe.[84] A single molecule SPECT/MR agent has also been reported that incorporates both ^{99m}Tc and Gd(III) into a heterotrimetallic array based on a DTPA core.[85] It should be noted that the large disparity in

sensitivity between MRI and PET means that the former requires a much higher dosage for *in vivo* imaging.

Radionuclide/optical probes

Dual radionuclide and optical imaging probes are typically dominated by fluorophore-functionalised PET/SPECT agents. However, lanthanide systems have much to offer in this context. For example, it is possible to couple Gd-DO3A-AM chelates to a ^{64}Cu porphyrin, potentially giving a trimodal MR(Gd)/PET(^{64}Cu)/optical(porphyrin) agent.[86] Of course it is also possible to imagine the combination of a luminescent lanthanide with a radioisotope (*e.g.* ^{18}F) labelled ligand architecture in a manner akin to the structures in Figure 25.

Comments and conclusions

The development of lanthanide coordination chemistry in the context of applied biological imaging has been profound. The unique magnetic and optical physical properties of the lanthanide ions have found great application in the design of probes that not only image, but can report on their local environment. Much of the chemistry associated with polyazacarboxylate Gd(III) MR contrast agents is mature (although the toxicity related problems of DTPA derivatives remains a concern), but some of the most interesting and imaginative developments now involve the design of multi-modal single molecule agents that incorporate Gd(III). Whilst Eu(III) dominates in the optical microscopy applications of lanthanide systems, optimisation of NIR emissive species, which offer the greatest potential in optical microscopy,

remains a challenge. However, advances in detection hardware and the use of multi-photon light sources may allow greater imaging depths to be achieved when moving from cells to tissue analysis.[4] Another area in which lanthanide ions can be expected to play an important role is in potential theranostic (*thera*py and diag*nostics*) agents, since the ability to image and deliver therapeutic action in a targeted manner will be of profound importance with respect to personalised healthcare.

Taken together a huge amount has been achieved with lanthanide ions thus far, and we hope that the selected examples presented in this review stimulate the interest for further reading. The future development of new agents for biomedical imaging, together with the development of new imaging techniques, will undoubtedly see lanthanide ions continue to play a pivotal role in the design of next generation imaging and therapeutic agents.

Acknowledgements

The authors thank Cardiff University for support.

References

[1] For general MRI: C.F.G.C. Geraldes, S. Laurent, *Contr. Med. Mol. Imag*., 2009, **4**, 1; P. Caravan, J.J. Ellison, T.J. McMurry, R.B. Lauffer, *Chem. Rev*., 1999, **99**, 2293; for general luminescence imaging: F. Lebond, S.C. Davis, P.A. Valdes, B.W. Pogue, *J. Photochem. Photobiol*. *B*, 2010, **98**, 77.
[2]E.J. New, D. Parker, D.G. Smith, J.W. Walton, *Curr. Opin. Chem. Biol*., 2010, **14**, 238; E. Terreno, D.D. Castelli, A. Viale, S. Aime, *Chem. Rev*., 2010, **110**, 3019.
[3] Recommended further reading in *Luminescence of Lanthanide Ions in Coordination Compounds and Nanomaterials*, A. de Bettencourt-Dias, Ed., Wiley 2014.
[4] http://www.nobelprize.org/nobel_prizes/chemistry/laureates/2014/
[5] For a comprehensive overview see J.R. Lakowicz, *Principles of fluorescence spectroscopy*, Springer, New York, 3rd Edn. 2006.

[6] S.A. Hilderbrand, R. Weissleder, *Curr. Opin. Chem. Biol.,* 2010, **14**, 71.
[7] a useful introduction to TPA fluorescence microscopy: P.T.C. So, C.Y. Dong, B.R. Masters, K.M. Berland, *Annu. Rev. Biomed. Eng*., 2000, **2**, 399.
[8] A. D'Aleo, A. Picot, P.L. Baldeck, C. Andraud, O. Maury, *Inorg. Chem*., 2008, 47, 10269.
[9] A. D'Aleo, G. Pompidor, B. Elena, J. Vicat, P.L. Baldeck, L. Toupet, R. Kahn, C. Andraud, O. Maury, *Chem. Phys. Chem*., 2007, **8**, 2125.
[10] A. Bourdolle, M. Allali, J-C. Mulatier, B. Le Guennic, J.M. Zwier, P.L. Baldeck, J-C. G. Bünzli, C. Andraud, L. Lamarque, O. Maury, *Inorg. Chem*., 2011, **50**, 4987.
[11] J-C. G. Bünzli, *Chem. Rev*., 2010, **110**, 2729.
[12] A. Mech, A. Monguzzi, F. Meinardi, J. Mezyk, G. Macchi, R. Tubino, *J. Am. Chem. Soc*., 2010, **132**, 4574.
[13] G. Mancino, A.J. Ferguson, A. Beeby, N.J. Long, T.S. Jones, *J. Am. Chem. Soc*., 2005, **127**, 524.
[14] S.J.A. Pope, *Polyhedron*, 2007, **26**, 4818.
[15] A. Beeby, I.M. Clarkson, R.S. Dickens, S. Faulkner, D. Parker, L. Royle, A.S. de Sousa, J.A. G. Willians, M. Woods, *J. Chem. Soc., Perkin Trans. 2*, 1999, 493.
[16] I. Hemmilä, *Applications of Fluorescence in Immunoassays*, 1st ed.; Wiley Interscience: New York, 1991.
[17] B. McMahon, P. Mauer, C.P. McCoy, T.C. Lee, T. Gunnlaugsson, *J. Am. Chem. Soc*., 2009, **131**, 17542.
[18] A. Beeby, S.W. Botchway, I.M. Clarkson, S. Faulkner, A.W. Parker, D. Parker, J.A.G. Williams, *J. Photochem. Photobiol. B*, 2000, **57**, 83.
[19] E. Deiters, B. Song, A-S. Chauvin, C.D.B. Vandevyver, F. Gumy, J-C.G. Bünzli, *Chem. Eur. J*., 2009, **15**, 1716.
[20] V. Fernández-Moreira, B. Song, V. Sivagnanam, A-S. Chauvin, C. D.B. Vandevyver, M. Gijs, I. Hemmilä, H-A. Lehr, J-C.G. Bünzli, *Analyst*, 2010, **135**, 42.
[21] C.P. Montgomery, B.S. Murray, E.J. New, R. Pal, D. Parker, *Acc. Chem. Res*., 2009, **42**, 925.
[22] G-L. Law, C. Man, D. Parker, J.W. Walton, *Chem. Commun*., 2010, **46**, 2391.
[23] D.G. Smith, G-L. Law, B.S. Murray, R. Pal, D. Parker, K-L. Wong, *Chem. Commun*., 2011, **47**, 7347.
[24] A. D'Aleo, A. Picot, A. Beeby, J.A. Gareth Williams, B. Le Guennic, C. Andraud, O. Maury, *Inorg. Chem*., 2008, **47**, 10258.
[25] A. D'Aleo, A. Picot, P.L. Baldeck, C. Andraud, O. Maury, *Inorg. Chem*., 2008, **47**, 10269.
[26] H.K. Kong, F.L. Chadbourne, G-L. Law, H. Li, H-L. Tam, S.L. Cobb, C-K. Lau, C-S. Lee, K-L. Wong, *Chem. Commun*., 2011, **47**, 8052.
[27] M. Soulie, F. Latzko, E. Bourrier, V. Placide, S.J. Butler, R. Pal, J.W. Walton, P.L. Baldeck, B. Le Guennic, C. Andraud, J.M. Zwier, L. Lamarque, D. Parker, O. Maury, *Chem. Eur. J*., 2014, **20**, 8636.
[28] S.J. Butler, L. Lamarque, R. Pal, D. Parker, *Chem. Sci*., 2014, **5**, 1750.
[29] A. Picot, A. D'Aleo, P.L. Baldeck, A. Grichine, A. Duperray, C. Andraud, O. Maury, *J. Am. Chem. Soc*., 2008, **130**, 1532.

[30] C.D.B. Vandevyver, A-S. Chauvin, S. Comby, J-C.G. Bünzli, *Chem. Commun*., 2007, 1716.
[31] B. Song, C.D.B. Vandevyver, A-S. Chauvin, J-C.G. Bünzli, *Org. Biomol. Chem*., 2007, **6**, 4125.
[32] S.V. Eliseeva, G. Auböck, F. van Mourik, A. Cannizzo, B. Song, E. Deiters, A-S. Chauvin, M. Chergui, J.-C.G. Bünzli, *J. Phys. Chem. B*, 2010, **114**, 2932.
[33] G. Lapadula, A. Bourdolle, F. Allouche, M.P. Conley, I. del Rosal, L. Maron, W.W. Lukens, Y. Guyot, C. Andraud, S. Brasselet, C. Coperet, O. Maury, R.A. Andersen, *Chem. Mat*., 2014, **26**, 1062.
[34] A. D'Aleo, A. Bourdolle, S. Brustlein, T. Fauquier, A. Grichine, A. Duperray, P.L. Baldeck, C. Andraud, S. Brasselet, O. Maury, *Angew. Chem. Int. Ed*., 2012, **51**, 6622.
[35] X. Wang, H. Chang, J. Xie, B. Zhao, B. Liu, S. Xu, W. Pei, N. Ren, L. Huang, W. Huang, *Coord. Chem. Rev*., 2014, **273-274**, 201, and thematically relevant review articles within the same volume.
[36] K. Hanaoka, K. Kikuchi, H. Kojima, Y. Urano, T. Nagano*, J. Am. Chem. Soc*., 2004, **126**, 12470.
[37] B. Song, G. Wang, M. Tan, J. Yuan, *J. Am. Chem. Soc*., 2006, **128**, 13442.
[38] M.P. Lowe, D. Parker, O. Reany, S. Aime, M. Botta, G. Castellano, E. Gianolio, R. Pagliarin, *J. Am. Chem. Soc*., 2001, **123**, 7601.
[39] B.K. McMahon, R. Pal, D. Parker, *Chem. Commun*., 2013, **49**, 5363.
[40] For example, C.M.G. dos Santos, A.J. Harte, S.J. Quinn, T. Gunnlaugsson, *Coord. Chem. Rev*., 2008, **252**, 2512.
[41] M.C. Heffern, L.M. Matosziuk, T.J. Meade, *Chem. Rev*., 2014, **114**, 4496.
[42] http://spectrum.ieee.org/biomedical/imaging/the-worlds-most-powerful-mri-takes-shape
[43] M. Botta, *Eur. J. Inorg. Chem*., 2000, 399.
[44] Assessment report EMA/740640/210 for European Medicines Agency.
[45] R.F. Reilly *Clin. J. Am. Soc. Nephrol.,* 2008, **3**, 747.
[46] M. Mikawa, H. Kato, M. Okumura, M. Narazaki, Y. Kanazawa, N. Miwa and H. Shinohara, *Bioconjugate Chem.,* 2001, **12**, 510.
[47] R. D. Bolskar, A.F. Benedetto, L.O. Husebo, R.E. Price, E.F. Jackson, S. Wallace, L.J. Wilson, J.M. Alford *J. Am. Chem. Soc.,* 2003, **125**, 5471.
[48] E. Toth, I. van Uffelen, L. Helm, A.E. Merbach, D. Ladd, K. Briley-Sæbø, K.E. Kellar, *Magn. Res. Chem*., 1998, **36**, S125.
[49] E. Toth, D. Pubanz, S. Vauthey, L. Helm, A.E. Merbach, *Chem. Eur. J*., 1996, **2**, 1607.
[50] E. Wiener, M.W. Brechbiel, H. Brothers, R.L. Magin, O.A. Gansow, D.A. Tomalia, P.C. Lauterbur, *Mag. Res. Med*., 2005, **31**, 1.
[51] R. Hovland, C. Gløgård, A. J. Aasen and J. Klaveness, *Org. Biomol. Chem*., 2003, **1**, 644.
[52] C. Gløgård, G. Stensrud, R. Hovland, S. L. Fossheim, J. Klaveness, *Intl. J. Pharm*., 2002, **233**, 131.
[53] Y. Yamakoshi, H. Qiao, A. N. Lowell, M. Woods, B. Paulose, Y. Nakao, H. Zhang, T. Liu, S. Lund-Katzh and R. Zhou, *Chem. Commun*., 2011, **47**, 8835.
[54] P. Gong, Z. Chen, Y. Chen, W. Wang, X. Wang and A. Hu, *Chem. Commun*., 2011, **47**, 4240.
[55] E. Gianolio, G.B. Giovenzana, D. Longo, I. Longo, I. Menegotto, S. Aime *Chem. Eur. J.,* 2007, **13**, 5785.

[56] A. H. Hung, M. C. Duch, G. Parigi, M. W. Rotz, L. M. Manus, D. J. Mastarone, K. T. Dam, C. C. Gits, K. W. MacRenaris, C. Luchinat, M. C. Hersam and T. J. Meade, *J. Phys. Chem. C*, 2013, **117**, 16263.
[57] K. Overoye-Chan, S. Koerner, R.J. Looby, A.F. Kolodziej, S.G. Zech, Q. Deng, J.M. Chasse, T.J. McMurry, P. Caravan *J Am Chem Soc.* 2008, **130**, 6025.
[58] A.D. Sherry, Y. Wu, *Curr. Opin. Chem. Biol*., 2013, 17, 167.
[59] V. Comblin, D. Gilsoul, M. Hermann, V. Humblet, V. Jacques, M. Mesbahi, C. Sauvage, J. F. Desreux, *Coord. Chem. Rev*., 1999, **185-186**, 451.
[60] V. Clementi and C. Luchinat *Acc. Chem. Res.*, 1998, **31**, 351.
[61] S. Aime, A.S. Batsanov, M. Botta, R.S. Dickins, S. Faulkner, C.E. Foster, A. Harrison, J.A.K. Howard, J.M. Moloney, T.J. Norman, D. Parker, L. Royle, J.A.G. Williams, *J.Chem. Soc., Dalton Trans.*, 1997, 3623.
[62] P. L. Anelli, I Bertini, M Fragai, L Lattuada, C Luchinat and G Parigi, *Eur. J. Inorg. Chem.*, 2000, 625.
[63] R. A. Moats, S. E. Fraser and T. J. Meade, *Angew. Chem. Intl. Ed.*, 1997, **36**, 726; A.Y. Louie, M.M. Huber, E.T. Ahrens, U. Rothbacher, R. Moats, R.E. Jacobs, S.E. Fraser, T.J. Meade, *Nat. Biotechnol.,* 2000, **18**, 321.
[64] E. Gianolio, J. Bhagavath Singh, M. Aswendt, F. Arena, A. Barge, M. Hoehn and S. Aime, *Proc. Intl. Soc. Mag. Reson. Med.,* 2010, 18.
[65] S. Aime, S. Geninatti Crich, M. Botta, G. Giovenzana, G. Palmisano and M. Sisti *Chem. Commun.*, 1999, 1577.
[66] R. Hovland, C. Gløgård, A. J. Aasen and J. Klaveness *J. Chem. Soc., Perkin Trans. 2*, 2001, 929.
[67] M. Andrews, A.J. Amoroso, L.P. Harding, S.J.A. Pope, *Dalton Trans*., 2010, **39**, 3407.
[68] K. Hanaoka, K. Kikuchi, Y. Uranoa and T. Nagano *J. Chem. Soc., Perkin Trans. 2*, 2001, 1840.
[69] J.L. Major, G. Parigi, C. Luchinat, and T.J. Meade, *Proc. Nat. Acad. Sci.*, 2007, **104**, 13881
[70] E.L. Que, C.J. Chang *J. Am. Chem. Soc.* 2006, **128**, 15942.
[71] E. Vinogradov, A.D. Sherry, R.E. Lenkinski, J. Mag. Res., 2013, 29, 155.
[72] S.D. Wolf, R.S. Balaban *Magn. Reson. Med.* 1989, **10**, 135; S. D. Wolff and R. S. Balaban, *J. Magn. Reson.* 1990, **86**, 164; K. M. Ward, A. H. Aletras, and R. S. Balaban *J. Magn. Reson.* 2000, **143**, 79.
[73] S. Zhang, M. Merritt, D.E. Woessner, R.E. Lenkinski, A.D. Sherry, *Acc. Chem. Res.*, 2003, **36**, 783.
[74] S. Aime, D.D. Castelli, E. Terreno, *Angew. Chem. Intl. Ed.*, 2002, **41**, 4334.
[75] S. Viswanathan, Z. Kovacs, K.N. Green, S.J. Ratnakar, A.D. Sherry, *Chem. Rev.*, 2010, **110**, 2960.
[76] S. Aime, D. Delli Castelli, E. Terreno, *Angew. Chem. Int. Ed.* 2005, **44**, 5513.
[77] C.S. Bonnet, E. Toth, *Comptes Rendus Chimie*, 2010, **13**, 700.
[78] L.E. Jennings, N.J. Long, *Chem. Commun*., 2009, 3511.
[79] A. Louie, *Chem. Rev*., 2010, **110**, 3146.
[80] F.L. Thorp-Greenwood, M.P. Coogan, *Dalton Trans*., 2011, 40, 6129.
[81] J.E. Jones, A.J. Amoroso, I.M. Dorin, G. Parigi, B.D. Ward, N.J. Buurma, S.J.A. Pope, *Chem. Commun*., 2011, **47**, 3374.

[82] C. Bernhard, C. Goze, Y. Rousselin, F. Denat, *Chem. Commun*., 2010, 46, 8267.
[83] C. Rivas, G.J. Stasiuk, J. gallo, F. Minuzzi, G.A. Rutter, N.J. Long, *Inorg. Chem*., 2013, **52**, 14284.
[84] L. Frullano, C. Catana, T. Benner, A. D. Sherry and P. Caravan, *Angew. Chem., Int. Ed*., 2010, **49**, 2382.
[85] J-A. Park, J.Y. Kim, H-K. Kim, W. Lee, S.M. Lim, Y. Chang, T-J. Kim, K.M. Kim, *ACS Med. Chem. Lett*., 2012, **3**, 299.
[86] C.P. Gros, A. Eggenspiller, A. Nonat, J-M. Barbe, F. Denat, *Med. Chem. Commun.*, 2011, **2**, 119.